

# Object Localization Using Deformable Templates

**Jonathan Michael Spiller**

A dissertation submitted to the Faculty of Engineering and the Built Environment,  
University of the Witwatersrand, Johannesburg, in fulfilment of the requirements for  
the degree of Master of Science in Engineering.

Johannesburg, April 2007

# Declaration

I declare that this dissertation is my own, unaided work, except where otherwise acknowledged. It is being submitted for the degree of Master of Science in Engineering in the University of the Witwatersrand, Johannesburg. It has not been submitted before for any degree or examination in any other university.

Signed this \_\_\_ day of \_\_\_\_\_ 20\_\_\_

---

Jonathan Michael Spiller.

# Summary

Object localization refers to the detection, matching and segmentation of objects in images. The localization model presented in this paper relies on deformable templates to match objects based on shape alone. The shape structure is captured by a prototype template consisting of hand-drawn edges and contours representing the object to be localized. A multistage, multiresolution algorithm is utilized to reduce the computational intensity of the search. The first stage reduces the physical search space dimensions using correlation to determine the regions of interest where a match is likely to occur. The second stage finds approximate matches between the template and target image at progressively finer resolutions, by attracting the template to salient image features using Edge Potential Fields. The third stage entails the use of evolutionary optimization to determine control point placement for a Local Weighted Mean warp, which deforms the template to fit the object boundaries. Results are presented for a number of applications, showing the successful localization of various objects. The algorithm's invariance to rotation, scale, translation and moderate shape variation of the target objects is clearly illustrated.

# Acknowledgements

I would like to thank the following people and cat for their assistance throughout this...ordeal:

Prof. Tshilidzi Marwala, my supervisor, for his moral and financial support, guidance, insight, inexhaustible (and believe me I tried) patience, and lunch.

My parents, for their love and support, for letting me move back in without paying rent. Ma, for proofreading this (I know how painful it was...I had to write it), and Dad, for the car keys.

Evan “Ed” Hurwitz, for sharing a lane with me or letting me solo mid, whichever was needed.

The folks at Kentron, for funding this research, and for not requiring phone calls (which I didn’t want to make), or emails (which I didn’t want to send).

Lynx, for keeping me company working late into the night, and for dfttt6666667777777777..... walking across my keyboard.

Charlene, for posing for the pictures. Without you I would have had to break my camera photographing Ed!

Angelina. Call me.

# Preface

This dissertation is presented to the University of the Witwatersrand, Johannesburg, South Africa, in fulfilment of the requirements of the degree of Master of Science in Engineering.

The dissertation is entitled “Object Localization Using Deformable Templates,” and complies with the university’s “paper-model” format. It consists of three chapters, each of which comprises a standalone paper written for submission to a conference or journal. These are:

1. J.M. Spiller and T. Marwala, “Object Localization Using Deformable Templates,” currently (on date of submission of this dissertation) being prepared for submission as a journal article.
2. J.M. Spiller and T. Marwala, “Evolutionary Algorithms for Warp Control Point Placement,” submitted to *The 2nd International Symposium on Intelligence Computation and Applications*, to take place in Wuhan, China, during September 2007.
3. J.M. Spiller and T. Marwala, “Medical Image Segmentation and Localization using Deformable Templates,” *In Proceedings of the International Federation of Medical and Biological Engineering*, 2006, Vol. 14, pp. 2176-2179, Springer-Verlag, Berlin Heidelberg, Eds. Sun I. Kim and Tae Suk Sah, ISSN: 1727-1983.

A fourth paper, “Object Localization in Aerial Images Using Deformable Templates,” is currently in the process of being written and has not been included in this document.

An extended abstract for this paper has been submitted to *The First International Symposium on Information and Computer Elements*, to take place during September 2007 in Kitakyushu, Japan. The paper details an application of the localization algorithm to aerial and satellite images and includes a section on predicting affine warps for template instantiations, based on photogrammetry and aerial geometry techniques.

# Contents

<b>Declaration</b>	<b>i</b>
<b>Summary</b>	<b>ii</b>
<b>Acknowledgements</b>	<b>iii</b>
<b>Preface</b>	<b>iv</b>
<b>Contents</b>	<b>vi</b>
<b>List of Figures</b>	<b>ix</b>
<b>Nomenclature</b>	<b>xii</b>
<b>1 Object Localization Using Deformable Templates</b>	<b>1</b>
1 Introduction . . . . .	3
2 Deformable Templates . . . . .	5
2.1 Free-Form Models . . . . .	6

2.2	Parametric Models . . . . .	7
3	The Deformation Model . . . . .	9
3.1	The Prototype Template . . . . .	10
3.2	Control Points . . . . .	11
4	The Multistage Algorithm . . . . .	12
4.1	Stage One - Regions of Interest . . . . .	13
4.2	Stage Two - Multiresolution Matching . . . . .	15
4.3	Stage Three - Template Warping . . . . .	20
5	Experimental Results . . . . .	29
5.1	Search Capability . . . . .	29
5.2	Template Convergence . . . . .	30
5.3	Rotation Invariance . . . . .	30
5.4	Scale Invariance . . . . .	31
5.5	Object Tracking . . . . .	31
6	Conclusion and Future Work . . . . .	32
	<b>References</b>	<b>39</b>
<b>2</b>	<b>Evolutionary Algorithms for Warp Control Point Placement</b>	<b>46</b>
1	Introduction . . . . .	47
2	Registration for Object Localization . . . . .	48

3	Template Warping . . . . .	49
4	Evolutionary Algorithms . . . . .	50
4.1	Genetic Algorithm . . . . .	51
4.2	Particle Swarm Optimization . . . . .	52
4.3	Simulated Annealing . . . . .	52
5	Results . . . . .	53
6	Conclusion . . . . .	55
	<b>References</b>	<b>56</b>
<b>3</b>	<b>Medical Image Segmentation and Localization Using Deformable Templates</b>	<b>57</b>
I	Introduction . . . . .	58
II	A Model of Deformation . . . . .	58
III	The Multi-Stage Algorithm . . . . .	58
IV	Experimental Results . . . . .	60
V	Conclusion . . . . .	61
	<b>References</b>	<b>61</b>

# List of Figures

<b>1</b>	<b>Object Localization Using Deformable Templates</b>	<b>1</b>
1	Deformable template model: (a) A prototype template of a Clownfish, with control points shown. (b) An image containing a Clownfish to be localized. . . . .	10
2	Defining shape: Different instances of objects with the same shape. . . . .	11
3	Finding the regions of interest: (a) Eye template. (b) Face image. (c) EPF obtained from (b). (d) NCC surface plot. (e) Binary image mask obtained by thresholding (d). (f) Regions of interest. . . . .	16
4	Edge Potential Fields: (a) Base image of Macaw. (b) Base edge map, $\sigma = 2$ . (c) Distance map, $\sigma = 2$ . (d) Base edge orientation map. . . . .	17
5	Multiresolution search: (a) Prototype Macaw template. (b) Coarse EPF, $\sigma = 4$ . (c) Medium EPF, $\sigma = 2.5$ . (d) Fine EPF, $\sigma = 1$ . (e) Final template match. (f) 5 Coarse EPF matches. (g) 3 Medium EPF matches. (h) 1 Fine EPF match. . . . .	20
6	Control point placement: (a) A prototype template of a hand. (b) Base image of a hand. (c) Template alignment showing initial (red) and optimized (green) control point locations. . . . .	22

7	LWM warping: (a) A prototype template of a hand. (b) A deformed template of the hand bending to the right. (c) A deformed template of the hand bending to the left. (d) Extreme deformation resulting in an impractical shape. . . . .	28
8	Search capability: (a) Prototype templates of the letters G O L F and the VW logo. (b) Image of Golf GTI. (c) Medium resolution localization showing spurious results, $E \approx 0.2$ . (d) Fine resolution localization, $E \approx 0.1$ . (e) Magnification of (c). (f) Magnification of (d). . . . .	34
9	Template convergence: (a) Image of a Snowy Owl overlaid with the prototype template, $E = 0.459$ . (b) Coarse resolution template warp, 20 iterations, $E = 0.317$ . (c) Medium resolution template warp, 50 iterations, $E = 0.223$ . (d) Fine resolution template warp, 100 iterations, $E = 0.086$ . . . . .	35
10	Rotation invariance: (a) Prototype template of windmill blade. (b) Image of windmill. (c) Localization of windmill blades at orientations around $360^\circ$ . (d) Magnified localization of windmill blades. . . . .	36
11	Scale Invariance: (a) Prototype arch template. (b) Image of the Segovia Aqueduct. (c) Localization of arches at various scales. (d) Magnified localization of arches. . . . .	37
12	Object Tracking: (a) Prototype hand template. (b) Frames showing hand motion. (c) Object tracking of hands within each frame. . . . .	38
<b>2</b>	<b>Evolutionary Algorithms for Warp Control Point Placement</b>	<b>46</b>
1	Average convergence characteristics of GA, PSO and SA. . . . .	54
2	Hand warp using GA: Image sequence showing initial to final template warps at 15 iteration intervals. . . . .	54
3	Fish warp using SA: Template warps at 0, 50, 75 iterations and final template localization. . . . .	55

4	Owl warp using PSO: Image sequence shows actual implementation of the localization algorithm at 0, 20, 50 and 100 iterations. . . . .	55
<b>3</b>	<b>Medical Image Segmentation and Localization Using Deformable Templates</b>	<b>57</b>
1	Deformable template matching: (a) A prototype template of a typical Corpus Callosum shape with control points. (b) MRI base image where the Corpus Callosum must be localized and segmented. . . . .	58
2	Corpus Callosum MRI images. (a) Original image. (b) Segmented image.	60
3	Segmentation of aneurysms in ultrasound images. . . . .	61
4	MRI lung segmentation. . . . .	61
5	Carpal bone segmentation from x-ray. . . . .	61

# Nomenclature

**EPF** - Edge Potential Field

**LWM** - Local Weighted Mean

**PSO** - Particle Swarm Optimization

**GA** - Genetic Algorithm

**SA** - Simulated Annealing

## Chapter 1

# Object Localization Using Deformable Templates

This paper forms the main body of the thesis, to which it also lends its name. It is currently (on date of submission of this dissertation) being prepared for submission as a journal article. It comprehensively details the template deformation model and the multistage algorithm, and presents a number of test results highlighting key features of the localization paradigm.

# Object Localization Using Deformable Templates

J.M. Spiller and T. Marwala

**Abstract-** A new algorithm is presented for localizing objects in images, using deformable templates. Prior knowledge of object shape is described by a prototype template, which consists of shape-representative contours and edges, as well as a set of control points for image warping. Computational efficiency is achieved using a multistage approach to find a match between the deformed template and objects in the image, by minimizing a cost function between the template and object boundary. The first stage of the algorithm reduces the physical search space size by determining the regions of interest using cross-correlation between the template and the edges of the image. A multiresolution paradigm is adopted for the second and third stages. In the second stage, an adapted hierarchical Chamfer matching scheme is used to find approximate matches between the template and the image using directional Edge Potential Fields (EPFs) of progressively higher resolutions. In the third stage, an innovative method using Particle Swarm Optimization is employed to find optimal control point placement at each resolution. A Local Weighted Mean (LWM) warp is also employed at this stage to facilitate a registration that iteratively deforms the template to fit these optimized points. The dimensionality of possible warp transformations is overcome by minimizing a cost function that penalizes extreme warps. The algorithm is successfully applied to a number of images and the localization results are given, with each test set highlighting a different aspect of the algorithm.

# 1 Introduction

Object localization refers to the location and retrieval of objects from complex images. It is a wide-ranging problem that has importance, both as a final outcome and as a preliminary stage, in many image processing and computer vision tasks. Typical applications include image database retrieval [1–3], object recognition [4,5], image segmentation [6,7] and registration [8,9]. In all such localization applications, *a priori* information in the form of an inexact model of an object needs to be matched to the objects present in the base image. This information typically includes properties such as shape, color, texture, etc.

This paper addresses the problem of localization based on objects' 2D shape information only. It is approached as a process of matching a deformable template to the object boundary in an input image. Prior knowledge of an object is defined by a binary template, which consists of a rough sketch of shape-representative contours and edges, as well as a set of control points for image warping. This prototype template is not parameterized, but complete shape information is contained in the bitmap image. In order to find objects similar in shape to the template, deformations of the prototype shape are required. Deformed templates are obtained by shifting the control points to generate varying parametric warp transforms.

In order to determine a match, a two term objective function is minimized. The first term measures the potential energy between the object boundary, specified by the deformable template, and the edges and gradient directions in the base image. During matching, this term attracts the template toward salient image features. The second term is a penalty function that penalizes extreme deformations and helps to maintain a likely shaped template. The localization model minimizes the objective function by iteratively adjusting the control point positions and then warping to find the lowest energy fit between the template and edges in the image.

The majority of non-rigid template matching techniques either require initialization near the final solution, or are too slow for practical use [10]. This is largely attributed to the fact that the number of possible transformations that can be applied to the template is very large, resulting in computationally intractable optimization requirements. In

contrast, the method presented here is able to quickly find a global optimal solution, without any initialization. The objective function that is minimized is non-convex, and in order to find its minima efficiently, a multistage, multiresolution algorithm is employed. In the first stage, regions of interest are determined by evaluating the 2D correlation between the template and the image. In the second stage, approximate matches between the template and the image are found using multiresolution directional EPFs. Template matches at coarse resolutions are used to initiate matching at finer ones. The final stage of the algorithm employs an innovative warping method that uses evolutionary algorithms to determine the placement of control points on the image, and then utilizes a LWM warp to deform the template to fit these points. Invariance to rotation, translation and scale is achieved by applying the template at discrete orientations during each stage.

The robustness of the algorithm is illustrated by experimental results showing the accurate detection of deformable shapes even in highly cluttered images. The algorithm presented here falls under the pattern theoretic model of Grenander [11, 12], and is based partially on the work of Zhong and Jain [13, 14], who have shown that localization paradigms such as this exhibit a number of important qualities [14]:

- They can match shapes that are curved or polygonal, closed or open, simply or multiply connected.
- They can retrieve objects based on shape information alone, even in complex images.
- They can localize objects independent of their location, orientation, size and number in the image.
- localization is achieved in a computationally efficient manner using a multistage, multiresolution approach.

The rest of this paper is set out as follows: Section 2 gives a brief review of deformable templates, discussing their background, different models and applications and the latest developments in the field. Section 3 defines the template model used by the presented algorithm. It discusses the prototype template and the control points used for warping. The multistage algorithm is detailed in Section 4. This section explains the three stages

of the matching technique, from the identification of regions of interest, through the multiresolution search, and lastly the template warping methodology. Section 5 contains the results for a number of test scenarios, with each experiment highlighting a different aspect of the algorithm. Finally, Section 6 gives a conclusion and presents a number of ideas for future work in this field.

## 2 Deformable Templates

Literature suggests that the first versatile technique for detection of parameterized shapes was proposed by Hough in 1962 [15]. Templates were described by a set of parameters such as the slope and intercept of a line. The Hough Transform (HT) transfers points from spatial space into parameter space, and then finds peaks in this new domain. The method was later improved by Rosenfeld, Ballard and Brown respectively, to detect shapes described by an analytic curve as well as to incorporate parameters to translate, rotate, and scale the template. [16–18]. Although it is relatively insensitive to noise and occlusion, the applicability of the HT is limited by excessive memory and computational requirements. It is also unreliable when tasked with finding deformed shapes, i.e. those that differ from the prototype by more complex transformations than translations, rotation and scale. Full surveys of the HT, its variants and its applications can be found in [19] and [20].

Deformable templates are referred to as “active” because of their ability to adjust to fit given data. Models of this type are useful because of their flexibility, and for their abilities to both impose geometric constraints on a shape, and integrate local image evidence [13]. Because of their wide-ranging application, substantial research on template modeling has been done in recent years. Current research can be divided into two categories:

- Free-form models.
- Parametric models.

This section provides a brief literature survey of influential free-form and parametric template models. A number of pioneering models are presented, as well as some of the

latest developments in the field.

## 2.1 Free-Form Models

Free-form models refer to models where no global structure is specified. Templates are constrained only by general regularization constraints such as smoothness and/or connectivity of the boundary. Free-form models are capable of representing any arbitrary shape, provided these constraints are satisfied. Templates of this kind are typically attracted to prominent image features by energy functions of some sort.

An early example of a free-form model is the elastic deformable model of [21]. This method establishes an elastic model of one of the two images to be matched, and then uses local forces to iteratively warp it towards the other image. In [22], this model was successfully extended to the 3D scenario. A popular free-form model known as an active contour was introduced by Kass, Witkin and Terzopoulos in 1988 [23, 24]. They presented an energy-minimizing spline, known as a “snake”, controlled by a combination of three forces that induce regularizing constraints to ensure smoothness, attract the snake to the desired features, and influence its shape if required. One weakness of snake models, however, is that they operate on local image information only. As such, they are susceptible to noise, and highly dependent on initial instantiation position. Numerous, varying provisions have been made to improve the robustness and stability of snakes. Notably, in [25], Cohen and Cohen introduced an inflationary “balloon” force to expand or contract the contour. This helped the snake to escape from local minima formed by spurious, weak image edges. Spline-based template models provide more structure than snake models. Templates are expressed as linear combinations of functions, such as B-spline basis, trigonometric basis and wavelets. Chan and Vese developed an active contour based on curve evolution and level sets to detect boundaries that are not clearly defined by gradient information [26].

A number of statistical methods have also been used to improve the robustness of template matching schemes. The authors of [27] used hierarchical eigen-shapes and Bayesian inference with Markov Chain Monte Carlo sampling to recover 3D shape and texture

of an object, based on a single 2D view. In [28], a Bayesian probability model of image filter-banks, sampled via Monte Carlo methods, was presented to overcome the requirements of an exhaustive search. B-splines were used in [29] to estimate parametric deformable contours. The authors formulated the problem in a statistical framework with the likelihood function being derived from a region-based image model.

Free-form models have been successfully applied to contour detection [23, 25], object tracking [30] and segmentation tasks [31]. Free-form models, however, do not inherently contain knowledge about the shapes they are finding. When such knowledge is available, it can be incorporated into the search using parametric deformable models.

## 2.2 Parametric Models

Parametric models are controlled using a set of parameters that encode specific shape characteristics as well as permissible deformations [13]. Models of this type are useful when specific shape information is known and can be described by the set of parameters. Parameterization is accomplished in one of two ways: It is done either by constructing a set of equations defining the curves in the shape, which can then be controlled by varying the equations' parameters, or by developing a prototype model and applying parametric transformations to it in order to obtain different deformations.

In the first instance - curve parameterization - all prior information is captured in analytic form, by equations that uniquely describe the constituent curves of a shape. As with free-form models, the curves evolve to fit the evidence by updating their parameters so as to minimize some curve energy function. In [32], parametric template models were used to locate road boundaries by searching for pairs of straight, parallel edges in radar images. In a facial feature detection application, eye and mouth templates were constructed using circles and parabolic curves and controlled by parameters such as the radius of the circle and the intercepts and stationary points of the parabolas [33]. The authors of [34] used elliptical Fourier descriptors to represent open and closed boundaries with high degrees of freedom, which matched objects in medical images. Distributions of Fourier coefficients were used to specify likely shapes, while a Bayesian likelihood was used to estimate the optimal object boundary. A similar scheme was used in [35],

but included region homogeneity and edge strength in the likelihood distribution. The applicability of curve parameterization is limited because shapes need to be well-defined *and* representable by a set of curves with a manageably small set of parameters.

In the second instance - prototype template modeling - parameterization is based on the pattern theory of Grenander [11,12], who developed a framework for representing classes of similar structure that are able to accommodate certain variability. Models of this type consist of a prototype template, which describes an overall architecture and shape, as well as a parametric mapping which governs variation of that shape. Templates are chosen based on prior knowledge of the shape, usually described by typical, expected or average shape and may even be learned from a set of training samples. The associated parametric mapping is chosen to reflect the particular deformations allowed in a specific application domain.

The basic idea of prototype-based deformable models can be traced back to 1973. In [36], Fischler and Elshlager used a number of rigid components, held together by springs to represent a scene. The springs served as constraints on the relative movements of the components, and the amount by which they stretched also provided a measure of the cost of a description. Also in 1973, Widrow used a template drawn on a “rubber sheet” that could be locally stretched to form a specific shape [37].

In [38], the authors used polygons to construct template models of human hands, and then used Markov processes to obtain variations of the prototype. Also involving hands, Amit *et al* [39] represented a prototype hand as an intensity image and used dynamic programming to obtain template variance. Training samples were used in [40] to compute the average shape of a class of objects for use as the prototype. The deformations of the templates were modeled by using linear combinations of eigenvectors obtained from the variations of the class individuals from the mean template.

More recently, Jain *et al* [14] used hand-drawn prototype templates, warped using radial basis functions to match objects in images. A Bayesian framework was adopted, basing the likelihood of a match on both the expected shape and image evidence. The author of [10] used triangulated polygons to approximate the boundaries of objects and then used dual graphs to embed each triangle independently in the image. The accuracy of

the match was evaluated based on the log-anisotropy measure of how far each embedding was from a similarity transform of that particular triangle.

As can be seen, the pattern theory of Grenander is extremely versatile because of the different choices for template type and deformation process [12].

### 3 The Deformation Model

The deformation model presented in this paper falls under the second class of parametric models. While sharing similarities with many of the prototype template models detailed, it also incorporates unique characteristics which can be adapted to suit various application domains. Based on the pattern-theoretic model of [11, 12], the proposed model comprises two parts. The first is a prototype template of the object to be matched, consisting of characteristic edges and contours. The second part of the model consists of a set of control points, defined on the template, that facilitates a parametric mapping of deformations of the prototype. This deformation is accomplished by a LWM transformation that preserves the smoothness of the template, as well as any contour connectivity that might exist. Matching is achieved by the optimization of a two term objective function similar to the Bayesian model used by [14]. The first term takes into account image information, and measures the potential energy between the template and the image. This is similar to a Bayesian likelihood. The second term takes into account prior shape information, and penalizes extreme warps of the prototype template using an elastic energy term. This is similar to a Bayesian prior. The first term is based on the models of [13, 14, 23, 41, 42] but, like [13, 14], it incorporates edge direction in addition to edge position to provide more robust localization capability. Where models under the Bayesian framework seek to maximize the posterior probability, this model seeks to minimize potential energy. This type of model is well suited to applications where inexact knowledge of the shape is available and the object can be represented by a template sketch. It also provides an advantage over the commonly used “snake” models, in that it inherently contains global structure and deformation information about the object, making it less susceptible to mismatches caused by weak image features. The model is extremely flexible and versatile, allowing different template selection and deformation

controls to be applied in different application domains. Figure 1 gives an example of a typical template sketch, with control points, along with an image containing the object to be localized.

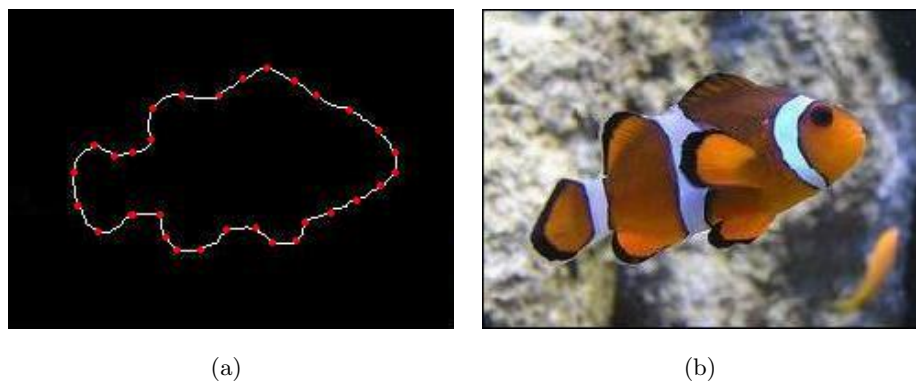


Figure 1: Deformable template model: (a) A prototype template of a Clownfish, with control points shown. (b) An image containing a Clownfish to be localized.

The definition for shape given in [43] states that: “Shape is all the geometrical information that remains when location, scale and rotational effects are filtered out from an object.” It is therefore required that an object localization scheme, based on shape, be invariant to changes in translation, scale and orientation, as well as acceptable deformations of the object [44]. Invariance to these characteristics is accomplished by utilizing specific, discrete template instances and orientations at each stage of the algorithm. Although effective, the requirement to test several discrete instances increases computational complexity, and is considered the main disadvantage with all template matching schemes [8]. Figure 2 shows an example of different objects with the same shape.

### 3.1 The Prototype Template

The prototype template is typically a hand-drawn sketch which describes the characteristic edges and contours of an object. It is captured as a binary, bitmap image with bright pixels (1s) on the contour, and dark pixels (0s) elsewhere. The contours defining the object shape need only be rough sketches and as such are under no constraints. In general, however, they should contain a number of high gradient edges in order to



Figure 2: Defining shape: Different instances of objects with the same shape.

represent only similarly shaped objects in an image [44]. Contours do not necessarily need to be closed or connected, and they may be comprised of several components. This flexibility allows the template to represent both the boundary and internal structure of the object. This template scheme captures the global structure of an object without requiring or specifying a parametric form for each shape class. It allows the embedding of *a priori* knowledge of object shape within an intuitive framework and has the further advantage that the amount of data is reduced significantly while retaining most of the image information. The inherent structure captured by the deformable template improves the algorithm's robustness in the incidence of weak, occluded or missing image features.

### 3.2 Control Points

The prototype template describes only a single, although most likely, instance of the object. In order to match similar objects in an image, a set of deformed templates is required. Therefore, in addition to the template sketch, the deformation model is specified along with a set of control points to be used for image warping. These control points, placed at desired coordinates on the template, act as anchors for a LWM transformation that can be applied to the prototype template to obtain deformations of the typical shape.

Control points in image registration applications are placed at distinct locations on the images. In [14], the authors used radial basis functions arranged in a grid pattern to facilitate image warping. LWM warping has the advantage that control points can be placed anywhere on the template. As such, expert knowledge of deformation can be incorporated into the model by placing control points to specifically aid the expected type of deformation. Landmarks such as vertices, midpoints, centroids and centers of mass are typical of expert knowledge [45], but LWM warping can also utilize control points placed in a grid pattern, or even at random. If control points are placed on the actual contour, the warp can be thought of as a bending of the contour at those specific points, whereas if the control points are placed randomly, or in a grid pattern, the warping can be visualised as the stretching of a 2D surface such as a rubber mat. Templates (edges and control points) may be obtained from training samples [46] or, as in this case, constructed from high-level, expert knowledge.

## 4 The Multistage Algorithm

One major problem of object localization algorithms is that of search space size. In typical applications, an object has to be retrieved regardless of translation, rotation and size. Given that the localization also needs to be invariant to partial shape changes in the target, this introduces a large number of variables to be determined during optimization. Objective functions of the type found in localization applications are typically not unimodal, and require a significant reduction of search space size in order to be computationally tractable [14]. A popular method used to accomplish the required search space reduction is to use a multiresolution algorithm. The algorithm presented in this paper takes the multiresolution approach one step further: it uses a multistage algorithm to reduce the search complexity by first reducing the physical size of the search space, and then iteratively reducing the number of variables to be optimized at each resolution.

The first stage of the algorithm is designed to reduce the physical size of the search space, the second stage to reduce the number of variables by determining likely values for template rotation, scale, and translation, and the third stage to determine the required warp deformation for the template. Although described separately, stages two and three

form the multiresolution segment of the algorithm and are performed repeatedly, one after the other, with an increase in resolution at each repetition.

#### 4.1 Stage One - Regions of Interest

In the first stage of the algorithm, the physical size of the search space is reduced by identifying regions in the image likely to provide a template match. This is accomplished using cross-correlation, a standard approach to feature detection. Cross-correlation between two images can be defined as a comparison of the two image signals at all possible relative positions [47]. It is used to measure the similarity between the template and the region of the image with which it is aligned. The image is essentially filtered with the template by convolving the two together and identifying regions where the overlapping template and image window share similar values.

The similarity between the template (T) and the base image (I) is evaluated by measuring the sum of the square of the differences between values in the template and the image. The sum of the squared Euclidean distance is given by [48]:

$$d_{T,I}^2(u, v) = \sum_{x,y}^N [T(x, y) - I(x - u, y - v)]^2 \quad (1)$$

Where the sum is taken over  $x, y$  for the  $N$  pixels of the template window positioned over the image at  $u, v$ . Equation 1 can be expanded to:

$$d_{T,I}^2(u, v) = \sum_{x,y}^N [T^2(x, y) - 2T(x, y)I(x - u, y - v) + I^2(x - u, y - v)]$$

or:

$$d_{T,I}^2(u, v) = \sum_{x,y}^N T^2(x, y) + \sum_{x,y}^N I^2(x - u, y - v) - 2 \sum_{x,y}^N T(x, y)I(x - u, y - v)$$

It can now be seen that the term  $\sum T^2(x, y)$  depends only on the template, and will be constant for every pixel in the image. The second term,  $\sum I^2(x - u, y - v)$ , is the sum of the square of the pixel values in the image that overlap the template. In images where the target object is well segmented from the background clutter, this remains

approximately constant for poorly matching regions [49]. The remaining term is twice the negative value of the correlation between  $T$  and  $I$ , and will increase as the Euclidean distance between them decreases. This yields the cross-correlation term which is used to measure the similarity between the template and the image window. It is given by [50]:

$$c(u, v) = \sum_{x,y}^N T(x, y)I(x - u, y - v) \quad (2)$$

This provides an intuitive method for using correlation to match a template to an image, since places where the correlation is high tend to be locations where the template and image match well.

Correlation provides simplicity in that it is shift invariant, meaning that the operation is unchanging for every pixel, and in that it is linear, replacing every pixel with a linear combination of its neighbors [50]. There are, however, a number of disadvantages to using (2) for template matching [49]:

- The range of  $c(u, v)$  is dependent on the size of the template.
- $c(u, v)$  is susceptible to changes in amplitude such as those caused by varying light conditions.
- In images where the target is not clearly segmented from a cluttered background, the image energy term,  $\sum I^2(x - u, y - v)$ , may vary with position. This may cause matching to fail, since high intensity regions may cause spurious correlation.

These problems can be overcome by normalising the template and image window vectors to unit length. This yields a cosine-like correlation coefficient, known as the normalised cross-correlation (NCC), given by [49]:

$$\gamma(u, v) = \frac{\sum_{x,y}^N [T(x, y) - \bar{T}][I(x - u, y - v) - \bar{I}_{u,v}]}{\left\{ \sum_{x,y}^N [T(x, y) - \bar{T}]^2 \sum_{x,y}^N [I(x - u, y - v) - \bar{I}_{u,v}]^2 \right\}^{\frac{1}{2}}} \quad (3)$$

Where  $\bar{T}$  is the mean of the template and  $\bar{I}_{u,v}$  is the mean of the image under the template window.

The peaks of the cross-correlation matrix occur where the template and image are best correlated. The NCC can be displayed as a surface plot or as an intensity image, the maxima of which are used to identify areas in the image where localization is likely to occur. The NCC is thresholded and dilated to isolate these areas, which are then transformed into a binary image mask. The mask overlaid on the image defines the regions of interest, forming the output of this stage of the algorithm.

NCC is not an ideal approach to feature matching, since it is not invariant with respect to scale, rotation, and deformation. However, these properties are overcome at least to some extent during this stage of the algorithm. Rotation invariance is achieved by calculating the NCC for a number of templates at discrete rotations. Moderate scale changes and deformations are accommodated by using an image’s EPF <sup>1</sup>, as opposed to the original image, as the  $I$  during NCC. The EPF “blurs” the edges of an image, essentially allowing for more relaxed matching requirements, while still maintaining robustness against spurious correlations. This is critical to the algorithm’s ability to locate objects with significant in-class shape variability. Stage one of the algorithm is graphically illustrated in Figure 3. This example finds the regions of interest for localizing an eye in an image of a face.

## 4.2 Stage Two - Multiresolution Matching

The second stage of the algorithm is tasked with finding approximate matches between the template and the structures within the image. This stage of the algorithm is based on the principle of sequential similarity detection [51], which dictates that full precision is needed only at the peaks of the correlation function, while reduced precision can be used elsewhere. Template matching is accomplished by use of a modified Chamfer matching technique [52].

Chamfer matching is an edge matching method, first proposed by Barrow *et al* [53], that attempts to find the best fit for edge points from two images by minimizing a generalized distance between them [44]. In a hierarchical Chamfer scheme, the matching is performed not only in the original image resolution, but in a series of images, where

---

<sup>1</sup>EPFs are detailed in the next section

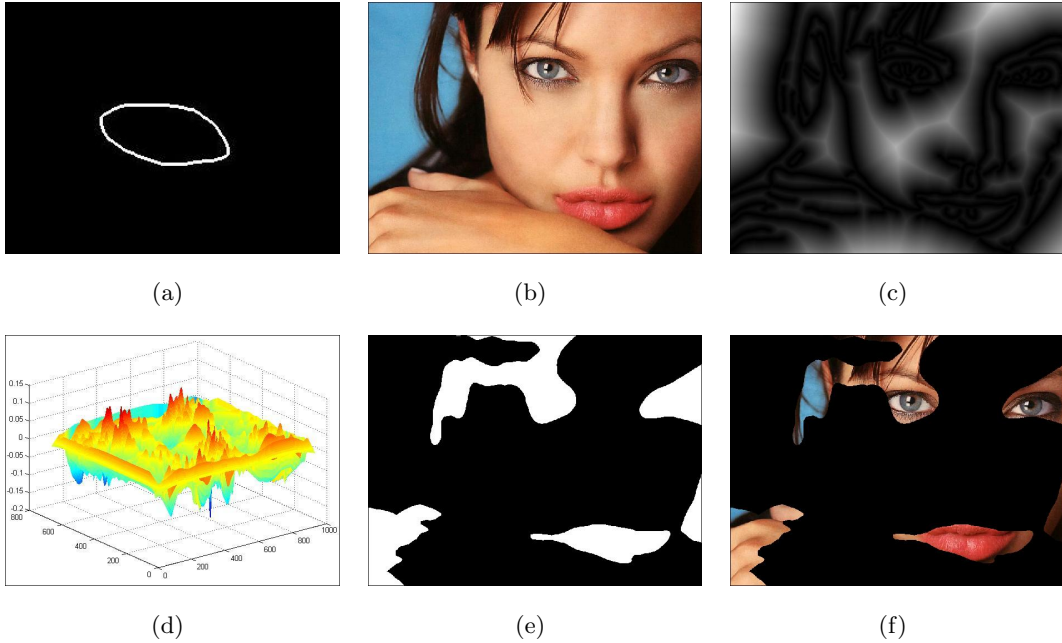


Figure 3: Finding the regions of interest: (a) Eye template. (b) Face image. (c) EPF obtained from (b). (d) NCC surface plot. (e) Binary image mask obtained by thresholding (d). (f) Regions of interest.

each image is a representation of the original scene at a lower resolution [52]. This stage of the algorithm operates under a multiresolution framework to locate the global optima within the regions of interest already identified by stage one, with regard for accuracy increasing with the resolution.

### Match Measure

The template is attracted and aligned to prominent image structures via directional EPFs, determined by the positions and orientations of edges in the image. The EP for an off (Binary 0) pixel  $(x, y)$  in the base edge map, obtained from the Euclidean distance transform, is defined by [14]:

$$\Phi(x, y) = -\exp\left\{-\rho\left(\delta_x^2 + \delta_y^2\right)^{\frac{1}{2}}\right\} \quad (4)$$

Where  $(\delta_x^2 + \delta_y^2)$  is the displacement from  $(x, y)$  to the nearest edge pixel. The smoothness of the potential field is controlled by the smoothing factor  $\rho$ . The EPFs are modified

to include a directional component for each pixel  $(x, y)$  in edge K by [54]:

$$\theta(x, y) = \arctan \left( \frac{\partial K(x, y)}{\partial y} / \frac{\partial K(x, y)}{\partial x} \right) \quad (5)$$

Figure 4 gives an example of a directional EPF. The base image of a Macaw parrot as well as its edge map are shown, along with the directional EPF which is comprised of a distance map, and an edge orientation map, colored to highlight the approximate edge directions. The edge map is found using a Canny edge detector [55].

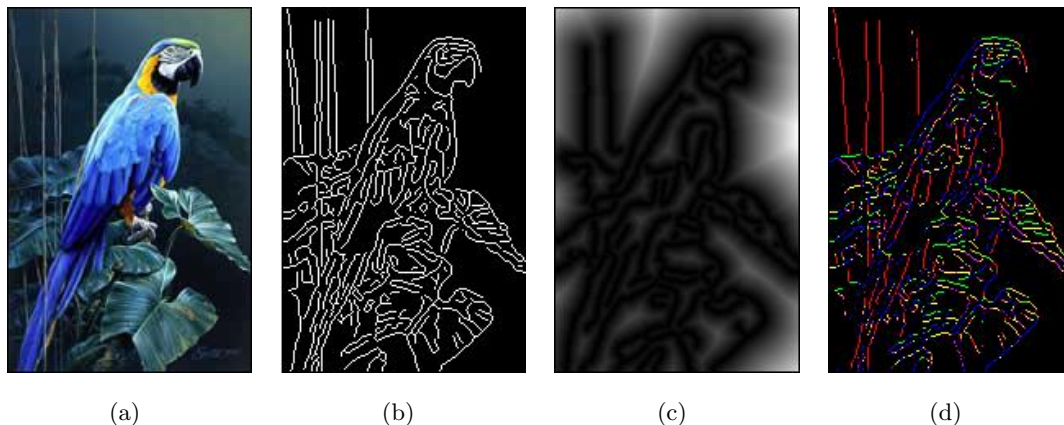


Figure 4: Edge Potential Fields: (a) Base image of Macaw. (b) Base edge map,  $\sigma = 2$ . (c) Distance map,  $\sigma = 2$ . (d) Base edge orientation map.

The modified directional edge potential yields the matching measure in the form of an energy function between the template and the base image, given by [14]:

$$E(T_{s,\theta,d,\zeta}, I) = \frac{1}{N_T} \sum_{i=1}^{N_T} \{1 + \Phi_i(x, y) |\cos [\beta(x, y)]|\} \quad (6)$$

Where the summation covers the  $N_T$  pixels on the template, and  $\beta(x, y)$  is the angle between the tangent of the base edge pixel *nearest*  $(x, y)$  and the tangent direction of the template *at*  $(x, y)$ . This energy measure, expressed as a correlation between the base image and the template deformed in terms of scale  $s$ , rotation  $\theta$ , displacement  $d$  and warp  $\zeta$ , is based on the Chamfer matching function but requires that the template agree with the image edges not only in position, but also in direction [14]. This requirement provides significantly improved robustness in noisy images. A perfect match yields an energy measure of  $E = 0$ .

High energy template matches are immediately discarded, while low energy templates (below an application-specific threshold) identified at this stage are now warped by stage three of the algorithm to fit the image features more accurately. After the warp, the energy function is re-evaluated and the warped templates are used as starting templates for progressively finer resolutions.

### Search Technique

The search for template matches is conducted by first finding approximate matches at the coarsest resolution, with little regard for matching accuracy, and then using these to initialize the search at progressively finer resolutions. At each resolution, the search is conducted by windowing a set of discrete template instances and orientations over the regions of interest in the image EPF and evaluating the match between them. Only templates with energy below an application-specific threshold are examined at increasing resolutions. Invariance to translation, rotation and scale is accomplished at this stage of the algorithm by using varied sets of discrete template instances and orientations at each resolution, with smaller step sizes between the discretizations at higher resolutions. Although often application dependent, typical discretizations as well as the match threshold required at each resolution are compared below.

#### Coarse Resolution:

Using the initial template  $T_i$ .

- **Rotation:** Templates are discretized to 12 orientations at  $30^\circ$  increments to span the range  $[0^\circ; 360^\circ]$ .
- **Translation:** These discretizations vary depending on the ratio of the template size to the image size,  $S_T : S_I$ . Typical windowing step size could be  $\frac{1}{4}S_T$ .
- **Scale:** Templates are discretized to 3 sizes. As percentages of the initial template size, these are  $70\%T_i$ ,  $100\%T_i$ ,  $130\%T_i$ .
- **Match Threshold:** Thresholds may vary depending on image types and applications. A typical threshold at this resolution would be  $E = 0.3$ .

**Medium Resolution:**

Using final template instances  $T_c$ , obtained from the coarse resolution warp.

- **Rotation:** Templates are discretized to 3 orientations of  $15^\circ$  increments to span the range  $[\theta(T_c) - 15^\circ; \theta(T_c) + 15^\circ]$ .
- **Translation:** Typical windowing step size could be  $\frac{1}{8}S_T$ .
- **Scale:** Templates are discretized to 3 sizes. As percentages of the coarse template size  $T_c$ , these are  $90\%T_c$ ,  $100\%T_c$ ,  $110\%T_c$ .
- **Match Threshold:** A typical threshold would be  $E = 0.2$ .

**Fine Resolution:**

Using final template instances  $T_m$ , obtained from the medium resolution warp.

- **Rotation:** Templates are discretized to 3 orientations at  $5^\circ$  increments to span the range  $[\theta(T_m) - 5^\circ; \theta(T_m) + 5^\circ]$ . Any rotation within this range is expected to be recovered by template deformation.
- **Translation:** Typical windowing step size could be  $\frac{1}{16}S_T$ .
- **Scale:** Template scales are not adjusted during this stage. Scale changes at this resolution are expected to be recovered by template deformation.
- **Match Threshold:** A typical threshold would be  $E = 0.1$ .

The multiresolution search is graphically illustrated in Figure 5. This example localizes the Macaw in Figure 4 using the prototype template shown. The coarse, medium and fine resolution EPFs are displayed along with the final template match and the approximate matches at each resolution from the intermediate search stages. The EPFs are obtained from the image edge maps, and their resolution is controlled by adjusting the standard deviation  $\sigma$  of the Gaussian filter used in the Canny edge detector. No warping of the template has been performed, and the displayed EPFs have undergone histogram equalization to enhance their clarity for the benefit of the reader.

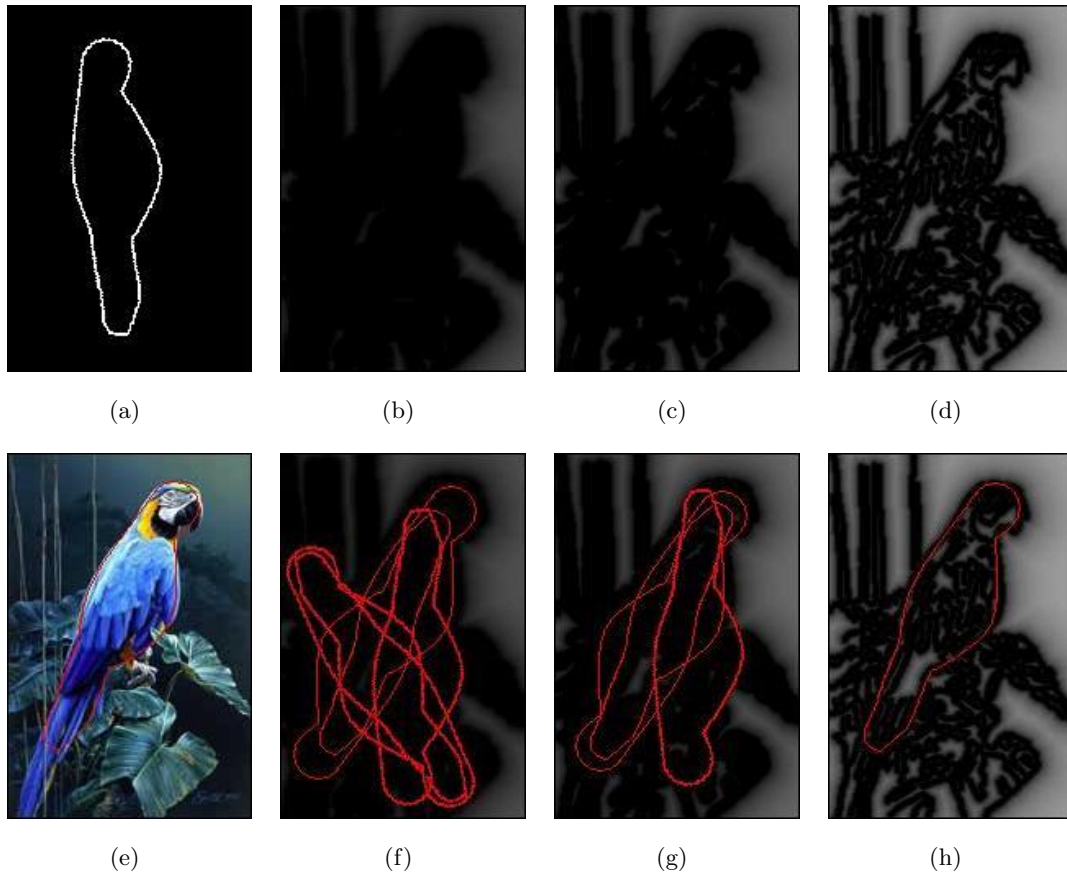


Figure 5: Multiresolution search: (a) Prototype Macaw template. (b) Coarse EPF,  $\sigma = 4$ . (c) Medium EPF,  $\sigma = 2.5$ . (d) Fine EPF,  $\sigma = 1$ . (e) Final template match. (f) 5 Coarse EPF matches. (g) 3 Medium EPF matches. (h) 1 Fine EPF match.

### 4.3 Stage Three - Template Warping

The prototype template describes only a single - although most likely - instance of the object shape [14]. In order to more accurately match objects in the image, this prototype has to be deformed to fit prominent edge features. Since the template image is to be matched to the base image as a final outcome of the warp, the deformation process can be considered as a registration between the template and the base image edge map.

Typical registration problems involve the overlaying of two images of the same scene, and require the determination of a set of corresponding control point positions on the two

images [45]. Once a correspondence between these control points has been established, they are used to determine a transformation function that maps the rest of the points in the image. Control point selection can be accomplished either manually or automatically. Manual selection may require high level, expert knowledge, while automatic methods typically rely on line intersections, locally maximum variances and curvatures or centers of gravity as control point positions. Control point placement for the warp used in this algorithm relies on a different approach, since the required control point locations on the base image are unknown. The previous two stages of the algorithm have been tasked with finding the regions of the global minima for localization, and the template locations identified in stage two are used as starting positions for this stage. As such, the templates are already partially aligned with the objects in the image and it can be assumed that a control point on the base image will be in approximately the same region as its corresponding control point on the template. Using this correspondence, the alignment between the template and the image can be refined, and the templates can be deformed to more accurately fit the image edges. The template warp  $\zeta$ , along with the stage two discretizations of rotation  $\theta$ , scale  $s$  and translation  $d$ , yield deformations of the prototype template  $T_0$  which are matched to the image using equation 6. The deformed templates are of the form [14]:

$$T_{s,\theta,d,\zeta}(x,y) = T_0 \{s \cdot [(x,y) + \zeta(R_\theta(x,y))] + (d_x, d_y)\} \quad (7)$$

## Particle Swarm Optimization

Particle Swarm Optimization, developed in 1995 by Dr Russel Eberhart and Dr James Kennedy, is a stochastic, population-based optimization method inspired by the social behaviour of flocking birds and schooling fish [56]. It is an evolutionary technique in which potential objective function solutions are modeled as particles in a swarm. These particles (also known as individuals) “fly” through the problem space following the current optimum particle [57]. During flight, each particle adjusts its trajectory towards the optimum, according to both its own experience and the experiences of its neighboring particles, making use of the best position encountered by itself and its neighbors. In this way, the whole swarm contributes to the solution of the problem [57]. The use of Particle Swarm optimization to determine control point placement is discussed here.

With the template overlaying the base image, the control point locations on the template are used to approximate sets of corresponding control points on the base edge map. These sets represent the individuals in the particle swarm. At each iteration of the swarm optimization, the control points within the sets are shifted and the template is warped to fit each set. This warp facilitates a registration between the deformed template and the base image. The accuracy of the registration is determined by once again measuring the energy between the now deformed template, and the base image edge map. The optimization can be run for a set number of iterations, or until some termination criteria, such as a minimum energy, is met. The Particle Swarm Optimization algorithm, its implementation and its application to control point placement, is detailed extensively in [58].

Figure 6 gives an example of control point placement. The hand template is overlaid with the base image and control points on the template are transferred to corresponding locations on the base (red control points). The Particle Swarm optimization algorithm iteratively adjusts these locations until the optimal positions are found (green control points).

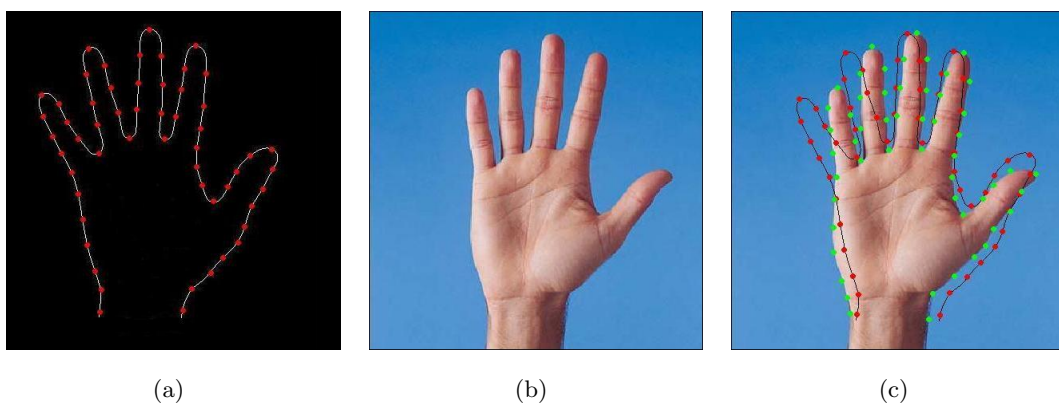


Figure 6: Control point placement: (a) A prototype template of a hand. (b) Base image of a hand. (c) Template alignment showing initial (red) and optimized (green) control point locations.

The use of Particle Swarm Optimization to determine optimal control point placement on the base image is effective because the regions of the global minima for localization have already been found by the first two stages of the algorithm. To prevent the

swarm from exploring outside these regions, as well as to limit warp dimensionality, a penalty function is introduced that penalizes extreme warps that would deform the template to impractical shapes. This function penalizes the Euclidean distance between corresponding control points on the template and base images, and ensures that during optimization, the swarm does not move the control points inordinate distances. The penalty function is added to the energy measure of equation 6. It is given by equation 8, where  $\alpha$  controls the rigidity of the warp. The initial  $\alpha$  is inversely proportional to the base image diagonal length, and is adjusted to reflect the expected variations in object shape. An increased  $\alpha$  is applied to rigid object structures and decreased  $\alpha$  to flexible ones.

$$P(x, y) = \alpha \sum_{i=1}^N \{(x_i - X_i)^2 + (y_i - Y_i)\}^{\frac{1}{2}} \quad (8)$$

### Defining a Warp Transformation Function

Inference of the appropriate transformation function is crucial to the accuracy of registration. Global transformations are typically used to register images that do not contain local geometric distortion [45]; however, template registration may require local geometric distortion depending on the local structure of the scene. The locally sensitive transformation function used for template warping in this algorithm is described here.

Given  $N$  corresponding control points  $(X_i, Y_i)$  on the template and  $(x_i, y_i)$  on the base image, the LWM warp requires two functions,  $X_i \approx f(x_i, y_i)$  and  $Y_i \approx g(x_i, y_i)$ , that approximate a mapping between these points as accurately as possible [45]. The problem is reformulated to give two sets of  $N$  3D points,  $(x_i, y_i, X_i)$  and  $(x_i, y_i, Y_i)$ , requiring the determination of the functions  $f$  and  $g$  [45]. The determination of the function  $f$  only is described here, since the function  $g$  can be determined in the same manner.

Given the set of  $N$  control points  $(x_i, y_i, X_i)$ , a transformation function is required such that when the coordinates of a control point on the base image are applied to it, it will approximate the  $X$ -component of the corresponding control point on the template.  $f$  is

typically taken to be a polynomial of order  $M$ , of the form [45, 59]:

$$f(x, y) = \sum_{j=0}^M \sum_{k=0}^j a_{jk} x^k y^{j-k} \quad (9)$$

The parameters  $a_{jk}$  of the polynomial can be determined using the least-squares method to minimize the error:

$$E = \sum_{i=1}^N [f(x_i, y_i) - X_i]^2 \quad (10)$$

Since this equation is a function of the parameters  $a_{jk}$ , its solution requires the determination of the partial derivatives of  $E$  with respect to each parameter. Solving for each partial derivative set equal to zero yields the system of linear equations known as the normal equations [60]:

$$\sum_{j=0}^M \sum_{k=0}^j a_{jk} \left[ \sum_{i=1}^N x_i^l y_i^{m-1} x_i^k y_i^{j-k} \right] = \sum_{i=1}^N X_i x_i^l y_i^{m-l} \\ l = 0, \dots, M; \quad m = 0, \dots, l. \quad (11)$$

## Incorporating Orthogonal Polynomials

The system described above consists of  $T = (M + 2)(M + 1)/2$  linear equations and is solvable provided  $N \geq T$ ; however, as  $T$  increases, the system becomes unstable and inaccurate. To avoid this, a set of  $N$  polynomials are constructed by the Gram-Schmidt orthogonalization process, using a set of linearly independent functions,  $h_i(x, y)$ , to have the form [61]:

$$\begin{aligned} P_0(x, y) &= a_{00} h_0(x, y) \\ P_1(x, y) &= a_{10} P_0(x, y) + a_{11} h_1(x, y) \\ P_2(x, y) &= a_{20} P_0(x, y) + a_{21} P_1(x, y) + a_{22} h_2(x, y) \\ &\vdots \\ P_T(x, y) &= a_{T0} P_0(x, y) + a_{T1} P_1(x, y) + \dots + a_{TT} h_T(x, y) \end{aligned} \quad (12)$$

Determination of parameters  $a_{jk}$  can now be accomplished by fixing values of  $a_{j0}$  and applying the following orthogonalization property to the polynomials [62]:

$$\sum_{i=1}^N P_k(x_i, y_i) P_l(x_i, y_i) = 0 \quad k \neq l. \quad (13)$$

If  $a_{j0} = 1$  is assumed for all values of  $j$ , then the parameters of the polynomials can be found using [62]:

$$a_{jj} = -\frac{\sum_{i=1}^N [P_0(x_i, y_i)]^2}{\sum_{i=1}^N P_0(x_i, y_i) h_j(x_i, y_i)}$$

$$j = 1, \dots, T.$$

$$a_{jk} = -a_{jj} \frac{\sum_{i=1}^N P_k(x_i, y_i) h_j(x_i, y_i)}{\sum_{i=1}^N [P_k(x_i, y_i)]^2}$$

$$j = 1, \dots, T; k = 1, \dots, T - 1. \quad (14)$$

Using a combination of orthogonal polynomials yields a transformation function [45]:

$$f(x, y) = \sum_{j=0}^T a_j P_j(x, y) \quad (15)$$

By substituting this new function into equation 10, once again solving for each partial derivative set equal to zero, and again applying the orthogonalization property of equation 13, it can be shown that the coefficients  $a_j$  can be found using [45]:

$$a_j = \frac{\sum_{i=1}^N X_i P_j(x_i, y_i)}{\sum_{i=1}^N [P_j(x_i, y_i)]^2} \quad (16)$$

As can be seen, if orthogonal polynomials are used, the solution of the system of equations is not required to determine the parameters of  $f$ . Another advantage of using orthogonal polynomials is that if the required accuracy of the transformation function changes, the required additional polynomials can simply be added to the system, without the need to recompute the old ones [45].

## Accounting for Local Geometric Difference

A disadvantage with using the least-squares method of error determination is that local geometric differences, as well as local control point inaccuracies, are averaged out equally over the whole image [45]. The effect of geometric difference and/or measurement inaccuracy is the same irrespective of how near or far the control point is to the approximating point. This is a highly undesirable property for a template warp that

requires local geometric distortion to achieve the required deformation. To localize the least-squares method, a weight function is defined that represents the influence of each  $i^{\text{th}}$  control on a point  $(x, y)$  by the inverse Euclidean distance between them. The weight function is given by [63]:

$$W_i(x, y) = [\delta + (x - x_i)^2 + (y - y_i)^2]^{-\frac{1}{2}} \quad (17)$$

Where  $\delta$  defines the influence of control points on the approximating point. The smaller the value of  $\delta$  the smaller the influence of distant control points, allowing a more local warp. Large values of  $\delta$  decrease the influence of nearby control points, allowing for a smoother warp.  $\delta$  also prevents the weight function from becoming infinite where  $x = x_i$  and  $y = y_i$ . As can be seen, different weights  $W_i(x, y)$  are obtained for different points  $(x, y)$  and can therefore be considered as a function of the position of points in the base image. By incorporating the weighting factor into the set of polynomials of equation 12 and again applying the orthogonalization property of equation 13, the parameters can be shown, through an adaptation of equation 14, to be given by [62]:

$$a_{jj}(x, y) = -\frac{\sum_{i=1}^N W_i(x, y)[P_0(x_i, y_i)]^2}{\sum_{i=1}^N W_i(x, y)P_0(x_i, y_i)h_j(x_i, y_i)}$$

$$j = 1, \dots, T.$$

$$a_{jk}(x, y) = -a_{jj}(x, y) \frac{\sum_{i=1}^N W_i(x, y)P_k(x_i, y_i)h_j(x_i, y_i)}{\sum_{i=1}^N W_i(x, y)[P_k(x_i, y_i)]^2}$$

$$j = 1, \dots, T; k = 1, \dots, T - 1. \quad (18)$$

Since the approximating transformation is still defined by equation 15, similarly to equation 16, the new coefficients  $a_j$  can be found using [45]:

$$a_j(x, y) = \frac{\sum_{i=1}^N W_i(x, y)X_iP_j(x_i, y_i)}{\sum_{i=1}^N [W_i(x, y)P_j(x_i, y_i)]^2} \quad (19)$$

### Local Weighted Mean Warp

Consider a point  $(x, y)$  in the base image, near to control point  $i$ . It is expected that the corresponding point on the template is also near to control point  $i$ . Therefore it

can be assumed that the  $X$  value of a point  $(x, y)$  may be determined by the  $X$  values of the nearby control points, according to an appropriate weighting function [45]. The transformation function, known as the weighted mean, is defined to have the form [64]:

$$f(x, y) = \frac{\sum_{i=1}^N W_i(x, y) X_i}{\sum_{i=1}^N W_i(x, y)} \quad (20)$$

Utilizing the weight definition of equation 17, this function generates a surface that passes through the  $N$  3D points  $(x_i, y_i, X_i)$  [64, 65]. The weighting function *favours* measurements from near points over distant ones, but still uses the entire measurement to determine the values of each point. This means that a local geometric distortion influences the deformation of the entire template image. In order to obtain a strictly local geometric warp, a transformation function is required that is influenced only by the appropriate 3D point and  $n - 1$  of its nearest neighbors [45]. This is accomplished by adapting the weighting function to be [45]:

$$\begin{cases} W_i(R) = 1 - 3R^2 + 2R^3 & 0 \leq R \leq 1. \\ W_i(R) = 0 & R \geq 1. \end{cases} \quad (21)$$

Where  $R = [\delta + (x - x_i)^2 + (y - y_i)^2]^{\frac{1}{2}} / R_n$  and  $R_n$  is the distance of point  $(x_i, y_i)$  from its  $(n - 1)^{th}$  nearest control point in the base image. This guarantees that polynomial  $i$  has no influence on points whose distance from control point  $(x_i, y_i)$  is larger than  $R_n$ . The weighted sum of the polynomials is continuous and smooth at all values of  $(x, y)$ , since [45]:  $[\frac{dW}{dR}]_{R=0} = [\frac{dW}{dR}]_{R=1} = 0$ . This yields the final transformation function which defines the  $X$  value (in the template) of an arbitrary point  $(x, y)$  (in the base image) by the weighted sum of polynomials having a non-zero weight over that point. The Local Weighted Mean function is given by [45, 66]:

$$f(x, y) = \frac{\sum_{i=1}^N W \left\{ [\delta + (x - x_i)^2 + (y - y_i)^2]^{\frac{1}{2}} / R_n \right\} P_i(x, y)}{\sum_{i=1}^N W \left\{ [\delta + (x - x_i)^2 + (y - y_i)^2]^{\frac{1}{2}} / R_n \right\}} \quad (22)$$

Where  $P_i(x, y)$  is the polynomial passing through point  $(x_i, y_i, X_i)$  and  $n - 1$  other points nearest to it.

LWM warping possesses a number of advantages over other warp methodologies [59]:

- **Orthogonal Polynomials:** As stated previously, the use of these allows for a component of the transformation to be obtained directly from the corresponding

control points, obviating the need for the solution of a system of equations. More polynomials can also be added as required, without the need to recompute the existing ones.

- **Approximate Transformation Functions:** Since corresponding control points are not mapped exactly to each other, digital errors in correspondence as well as mismatch errors are automatically accounted for and smoothed by the warp.
- **Adaptive Weight Functions:** The rational weight functions adapt to the locations and densities of the control points. They automatically extend to sparsely populated areas and increase or decrease in width according to the spacing between the points. This removes the stringent accuracy requirements typical of control point selection, and makes it possible to warp templates where the density of the points varies considerably in the image domain. The width of the weight functions can also be globally controlled to vary the smoothness or rigidity of the warp.

An example set of warped templates is shown in Figure 7. The first two of the deformed templates are likely candidates for a match, while the third is too warped to be of practical use. This last template would be excluded before creation, by the penalty function (equation 8) operating on the control point locations.

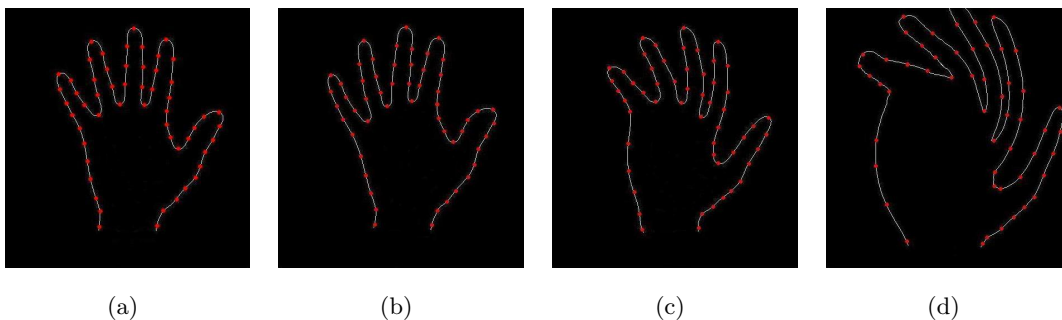


Figure 7: LWM warping: (a) A prototype template of a hand. (b) A deformed template of the hand bending to the right. (c) A deformed template of the hand bending to the left. (d) Extreme deformation resulting in an impractical shape.

## 5 Experimental Results

The localization algorithm presented in this paper has been applied to a variety of different objects in several images. Results are given for a number of test applications and have been divided into five categories, each illustrating a different aspect of, and highlighting different capabilities of, the algorithm.

The experimental results presented here vary considerably with respect to a number of important features. Background clutter in an image influences the effectiveness of the cross-correlation results from stage one. Image and template sizes, as well as the ratio of the template size to the image size  $S_T : S_I$  for each application define how long a particular multiresolution search will take. The complexity of the required template warp changes the iteration requirements for the Particle Swarm optimization and the LWM warp. The code platform (Matlab<sup>TM</sup> in this case) also greatly affects computation time. A comparative study of these factors is therefore not useful. The time per localization varies between approximately 5s for low  $S_T : S_I$  and 40s for high.

With the exception of the section regarding scale invariance, all template images have all been enlarged for clarity.

### 5.1 Search Capability

The first category of experiments illustrates the search capability of the algorithm, highlighting the translation invariance of the localization scheme. The multistage, multiresolution approach is used to automatically locate objects of interest within the given image. A number of small (relative to the image size) objects of different shapes are localized independently using different prototype templates. The algorithm is able to search a complex image and successfully identify the required objects. The search capability of the algorithm is highlighted in Figure 8.

Figure 8a shows five independent templates for the letters **G O L** and **F** as well as for the VW logo. These template structures are to be identified in Figure 8b. Figure 8c (and the magnification in Figure 8e) shows the localization results at the medium

resolution, showing the spurious localization of the vehicle’s front right lights and the **T** in the licence plate (from the **F** template). However, at the fine resolution level of Figure 8d (and the magnification in Figure 8f), the correct localization is achieved.

This experiment also illustrates two further properties of the algorithm. It shows that the algorithm can localize complex shapes using multiply-connected templates with internal structure (VW logo), and highlights the ability of the algorithm to identify text within images. By noting which templates successfully localize letters (and at what locations), text can effectively be read by the algorithm.

## 5.2 Template Convergence

The second category of experiments demonstrates the warp capability of the algorithm, and shows how the templates are able to locally deform to match the objects in the image. The template is initially overlaid on the coarse resolution image EPF , and is shifted to obtain the best match. Particle Swarm optimization is then used to warp the template to fit the object features before increasing the resolution and repeating the process.

Figure 9 shows the deformation process for localizing a Snowy Owl. The prototype template match as well as snapshots of the final deformed templates at each resolution are presented to illustrate how the template evolves to match the salient object structures. The object is correctly retrieved and template convergence toward the object contours can be seen clearly.

## 5.3 Rotation Invariance

The aim of the third category of experiments is to demonstrate the rotation invariance of the localization algorithm. This is accomplished by utilizing a set of discrete template instances to find objects at different rotations.

Figure 10 shows the localization of windmill blades at orientations around  $360^\circ$ . To be noted in the magnified image of Figure 10c, is the occurrence of two spurious localizations

of windmill blades at the bottom of the windmill circle (approximately  $260^\circ$  and  $280^\circ$ ). These are due to the edges of windmill base providing the required structure for localization. Scale invariance was removed from the algorithm for this experiment by restricting the template scale to the original size. This was done to exclude the localizations of the windmill blade shape within the windmill strut.

This experiment also illustrates the algorithm's ability to identify multiple instances of the same object. Since this is an inherent property of the search technique, apart from having to examine these additional matches more closely at each resolution, no additional computational overhead is involved (this is not true of warping the template to fit multiple objects).

## 5.4 Scale Invariance

Category four experimentation results illustrate the scale invariance of the localization scheme. This is demonstrated by localizing multiple objects of similar shape but varying scale, using a set of discrete template instances that are scaled versions of the original.

Figure 11 shows the localization of Arches in the Segovia Aqueduct, using the prototype template shown. The original template is used to localize the arches at the top right of the image, and a "slanted" affine warp of the original template is used to generate templates for the narrower arches. The smaller arches in the center of the bottom row are localized using 25% and 50% scaled versions of the original template. Multiple scaled localizations are correctly retrieved in this manner.

## 5.5 Object Tracking

The fifth category of experiments highlights a consequential property of the localization algorithm, that of object tracking.

The images in Figure 12 show four different hand images, each slightly different from the next in terms of both shape and orientation. By first using the prototype template to localize the hand in the first frame of Figure 12b, and then using the final template from

each image as the prototype template for the subsequent one, the hand can be tracked through the four frames. The use of evolving prototype templates allows the algorithm to accommodate the variations in shape of the hands in each image.

Although the inherent properties of the localization algorithm allow it to track simple objects by performing a full localization on each frame, it is not as efficient or as effective as dedicated template tracking schemes that use additional image cues such as region consistency and interframe motion to reduce computational complexity [67]. This set of experiments also illustrates the fact that the localization algorithm can handle prototype templates that consist of open contours.

## 6 Conclusion and Future Work

An algorithm has been presented for the localization of objects in images using deformable templates. The deformable model consists of a hand-drawn, prototype template intended to capture *a priori* knowledge about the object shape, as well as a set of control points on the template. These points are used in a LWM warp to obtain deformations of the object shape. A multistage, multiresolution algorithm has been presented, detailing the different stages used in the search and matching process. The algorithm reduces computational complexity by first using cross-correlation to reduce the physical size of the search space, and then reducing the number of variables to be optimized at each stage using an adapted, hierarchical Chamfer matching scheme. Warping is accomplished as a registration between the template and the image, using Particle Swarm optimization to locate the optimal control point locations. Test results for a number of images have been given, with each set of results highlighting a different aspect, and different capabilities, of the algorithm. The quality of the results is a consequence of the combination of a search technique that can efficiently find a global optimal solution to the non-rigid matching problem, and a warping method that inherently takes advantage of the prior shape knowledge.

Future work in this field could proceed along, *inter alia*, the following lines:

- The algorithm could be adapted to include image attributes other than shape alone.

Properties such as interior and exterior or background and foreground intensities, region homogeneity, color and texture, could be utilized to improve the accuracy of the match and speed up the search process.

- The algorithm could be adapted to object tracking. The algorithm would operate under the same multistage approach as the one presented, but would include image cues specific to tracking tasks. These could include interframe motion, where the boundary of a moving object is characterised by large interframe differences, and region consistency, based on the premise that an object would retain a consistent color and texture throughout the frame sequence. Neural networks could also be incorporated to predict the typical path of an object.
- The algorithm could be adapted to a 3D environment. Pixels would become voxels and the search, matching and warping would be conducted in 3D space. This may require significant adaptation of certain sections of the algorithm, such as the cross-correlation used to determine regions of interest, the cost of which becomes prohibitive in three dimensions.



(a)



(b)



(c)



(d)



(e)

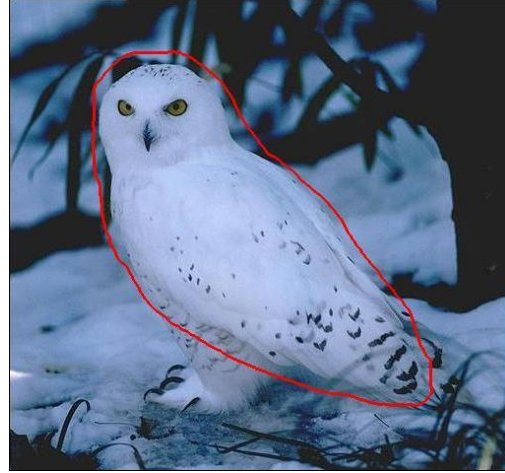


(f)

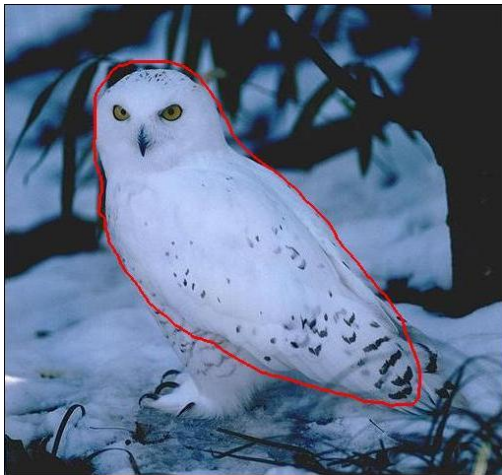
Figure 8: Search capability: (a) Prototype templates of the letters G O L F and the VW logo. (b) Image of Golf GTI. (c) Medium resolution localization showing spurious results,  $E \approx 0.2$ . (d) Fine resolution localization,  $E \approx 0.1$ . (e) Magnification of (c). (f) Magnification of (d).



(a)



(b)

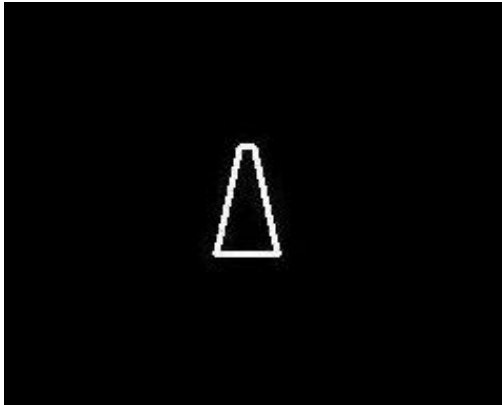


(c)



(d)

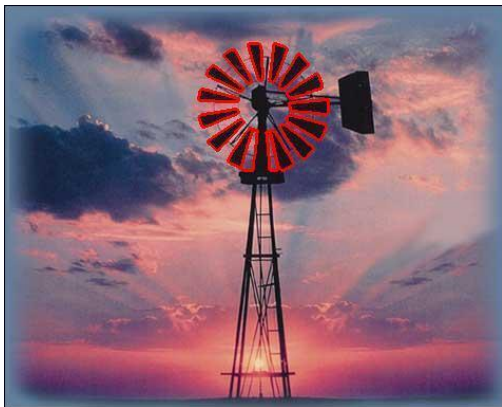
Figure 9: Template convergence: (a) Image of a Snowy Owl overlaid with the prototype template,  $E = 0.459$ . (b) Coarse resolution template warp, 20 iterations,  $E = 0.317$ . (c) Medium resolution template warp, 50 iterations,  $E = 0.223$ . (d) Fine resolution template warp, 100 iterations,  $E = 0.086$ .



(a)



(b)

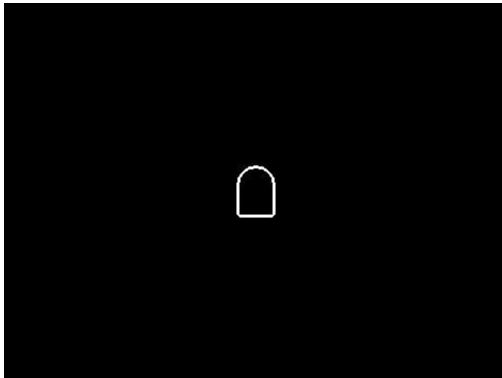


(c)



(d)

Figure 10: Rotation invariance: (a) Prototype template of windmill blade. (b) Image of windmill. (c) Localization of windmill blades at orientations around  $360^\circ$ . (d) Magnified localization of windmill blades.



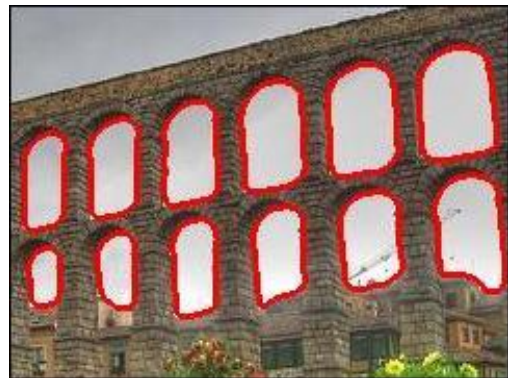
(a)



(b)



(c)



(d)

Figure 11: Scale Invariance: (a) Prototype arch template. (b) Image of the Segovia Aqueduct. (c) Localization of arches at various scales. (d) Magnified localization of arches.



(a)



(b)



(c)

Figure 12: Object Tracking: (a) Prototype hand template. (b) Frames showing hand motion. (c) Object tracking of hands within each frame.

# References

- [1] C. Faloutsos, R. Barber, M. Flicker, J. Hafner, W. Niblack, and W. Equitz, “Efficient and Effective Querying by Image Content,” *Journal of Intelligent Information Systems*, vol. 3, no. 3, pp. 231–262, 1994.
- [2] T. Kato, “Database Architecture for Content-Based Image Retrieval,” *In Proceedings of the SPIE - The International Society for Optical Engineering*, vol. 1662, pp. 112–123, 1992.
- [3] B. Holt and L. Hartwick, “Visual Image Retrieval for Applications in Art and Art History,” *Proc. SPIE*, vol. 2185, pp. 70–81, February 1994.
- [4] A. Yuille, “Deformable Templates for Face Recognition,” *Journal of Cognitive Neuroscience*, vol. 3, no. 1, pp. 59–70, 1991.
- [5] M. P. Dubuisson-Jolly, S. Lakshmanan, and A. K. Jain, “Vehicle Segmentation and Classification Using Deformable Templates,” *PAMI*, vol. 18, no. 3, pp. 293–308, March 1996.
- [6] D. Rueckert and P. Burger, “Geometrically Deformable Templates for Shape-Based Segmentation and Tracking in Cardiac MR Image,” *Proceedings of the International Workshop on Energy Minimization Methods in Computer Vision and Pattern Recognition*, pp. 83–98, 1997.
- [7] F. Poupon, J. F. Mangin, D. Hasboun, C. Poupon, I. Magnin, and V. Frouin, “Multi-object Deformable Templates Dedicated to the Segmentation of Brain Deep Structures,” in *Proceedings of the First International Conference on Medical Image*

*Computing and Computer-Assisted Intervention (MICCAI '98)*, M. Wells, Ed., vol. LNCS, no. 1496. Berlin, Heidelberg: Springer-Verlag, 1998, pp. 1134–1143.

- [8] E. Suárez, C. F. Westin, E. Rovaris, and J. Ruiz-Alzola, “Nonrigid Registration Using Regularized Matching Weighted by Local Structure,” in *Proceedings of the Fifth International Conference on Medical Image Computing and Computer-Assisted Intervention (MICCAI '02)*, T. Dohi and R. Kikinis, Eds., vol. LNCS, no. 2489. Berlin, Heidelberg: Springer-Verlag, 2002, pp. 581–589.
- [9] S. K. Warfield, M. Kaus, F. A. Jolesz, and R. Kikinis, *Medical Image Computing and Computer-Assisted Intervention - MICCAI'98: First International Conference*. Springer Berlin / Heidelberg, W.M. Wells and A. Colchester and S. Delp, Eds., 1996, vol. 1496, ch. Adaptive Template Moderated Spatially Varying Statistical Classification, p. 431.
- [10] P. Felzenszwalb, “Representation and Detection of Shapes in Images,” Ph.D. dissertation, Massachusetts Institute of Technology, September 2003.
- [11] U. Grenander, “Pattern Synthesis: Lectures in Pattern Theory,” *Applied Mathematical Sciences*, vol. 18, Springer-Verlag, 1976.
- [12] U. Grenander and D. M. Keenan, *Towards Automated Image Understanding, Advances in Applied Statistics: Statistics and Images*. Carfax Publishing Company, 1993, vol. 1, ch. 6, pp. 89–103.
- [13] Y. Zhong, “Object Matching Using Deformable Templates,” PhD Thesis, Department of Computer Science, Michigan State University, 1997.
- [14] A. K. Jain, Y. Zhong, and S. Lakshmanan, “Object Matching Using Deformable Templates,” *IEEE Transactions on Pattern Analysis and Machine Intelligence*, vol. 18, no. 3, pp. 267–278, MARCH 1996.
- [15] P. V. C. Hough, “Methods and Means for Recognising Complex Patterns,” U.S. Patent 3069654, Tech. Rep., 1962.
- [16] A. Rosenfeld, “Picture Processing by Computer: Survey,” *Surveys*, vol. 1, no. 3, pp. 147–176, September 1969.

- [17] D. H. Ballard, “Generalizing the Hough Transform to Detect Arbitrary Shapes,” *Pattern Recognition*, vol. 13, pp. 111–122, 1981.
- [18] D. H. Ballard and C. M. Brown, *Computer Vision*. Englewood Cliffs, NJ: Prentice-Hall, 1982.
- [19] J. Illingworth and J. Kittler, “A Survey of Hough Transform,” *CVGIP*, vol. 44, pp. 87–116, 1988.
- [20] V. Leavers, “Survey: Which Hough transform?” *CVGIP: Image Understanding*, vol. 58, pp. 250–264, 1993.
- [21] D. J. Burr, “Elastic Matching of Line Drawings,” *IEEE Transactions on Pattern Analysis and Machine Intelligence*, vol. 3, no. 2, pp. 708–713, November 1981.
- [22] M. Moshfeghi, S. Ranganath, and K. Nawyn, “Three-Dimensional Elastic Matching of Volumes,” *IEEE Transactions on Pattern Analysis and Machine Intelligence*, vol. 3, no. 2, pp. 128–138, March 1994.
- [23] M. Kass, A. Witkin, and D. Terzopoulos, “Snakes: Active Contour Models,” *IJCV*, vol. 1, no. 4, pp. 321–331, 1988.
- [24] D. Terzopoulos, A. Witkin, and M. Kass, “Constraints on Deformable Models: Recovering 3D Shape and Nonrigid Motion,” *AI*, no. 36, pp. 91–123, 1988.
- [25] L. Cohen and I. Cohen, “Finite-Element Methods for Active Contour Models and Ballons for 2-D and 3-D Images,” *IEEE Transactions on Pattern Analysis and Machine Intelligence*, vol. 15, no. 11, pp. 1131–1147, November 1993.
- [26] T. F. Chan and L. A. Vese, “Active Contours Without Edges,” *IEEE Transactions on Image Processing*, vol. 12, no. 2, pp. 266–277, February 2001.
- [27] T. Kostiainen, I. Kalliomäki, T. Tamminen, and J. Lampinen, “3D Object Recognition Based on Hierarchical Eigen Shapes and Bayesian Inference,” in *Proc. SPIE Vol. 4572, p. 165-173, Intelligent Robots and Computer Vision XX: Algorithms, Techniques, and Active Vision*, D. P. Casasent and E. L. Hall, Eds., vol. 4572, October 2001, pp. 165–173.
- [28] J. Sullivan, A. Blake, M. Isard, and J. MacCormick, “Bayesian Object Localisation in Images,” *IJCV*, vol. 44, no. 2, p. 111135, 2001.

- [29] M. A. T. Figueiredo, J. M. N. Leito, and A. K. Jain, “Unsupervised Contour Representation and Estimation Using B-Splines and a Minimum Description Length Criterion,” *IEEE Transactions on Image Processing*, vol. 9, no. 6, pp. 1075–1087, June 2001.
- [30] F. Leymarie and M. D. Levine, “Tracking Deformable Objects in the Plane Using an Active Contour Model,” *IEEE Transactions on Pattern Analysis and Machine Intelligence*, vol. 15, no. 6, p. 617634, June 1993.
- [31] A. Witkin, D. Terzopoulos, and M. Kass, “Signal Matching Through Scale Space,” *International Journal of Computer Vision*, pp. 133–144, 1987.
- [32] S. Lakshmanan and D. Grimmer, “A Deformable Template Approach to Detecting Straight Edges in Radar Images,” *IEEE Transactions on Pattern Analysis and Machine Intelligence*, vol. 18, no. 4, pp. 438–443, April 1996.
- [33] A. L. Yuille, P. Hallinan, and D. Cohen, “Feature Extraction from Faces Using Deformable Templates,” *International Journal of Computer Vision*, vol. 8, no. 2, pp. 133–144, 1992.
- [34] L. Staib and J. Duncan, “Boundary Finding with Parametrically Deformable Models,” *IEEE Transactions on Pattern Analysis and Machine Intelligence*, vol. 14, no. 11, pp. 1061–1075, November 1992.
- [35] A. Chakraborty, L. Staib, and J. Duncan, “Deformable Boundary Finding Influenced by Region Homogeneity,” *Proceedings of the IEEE conference on Computer Vision and Pattern Recognition*, pp. 624–627, June 1994.
- [36] M. A. Fischler and R. A. Elschlager, “The Representation and Matching of Pictorial Structures,” *IEEE Transactions on Computers*, vol. 22, no. 1, pp. 67–92, 1973.
- [37] B. Widrow, “The Rubber Mask Technique, Parts I and II,” *Pattern Recognition*, vol. 5, pp. 175–211, 1973.
- [38] U. Grenander, Y. Chow, and D. M. Keenan, *Hands: a Pattern Theoretic Study of Biological Shapes*. New York, NY, USA: Springer-Verlag New York, Inc., 1991.

- [39] Y. Amit, U. Grenander, and M. Piccioni, "Structural Image Restoration Through Deformable Templates," *American Statistical Association Journal*, vol. 86, no. 414, pp. 376–387, 1991.
- [40] T. Cootes, C. Taylor, and A. Lanitis, "Active Shape Models: Evaluation of a Multiresolution Method for Improving Image Searches," *Proceedings of the British Machine Vision Conference*, vol. 1, pp. 327–336, 1994.
- [41] M. A. T. Figueiredo and J. M. N. Leito, "Bayesian Estimation of Ventricular Contours in Angiographic Images," *IEEE Transactions on Medical Imaging*, vol. 11, no. 11, pp. 416–429, September 1992.
- [42] G. Storvik, "A Bayesian Approach to Dynamic Contours Through Stochastic Sampling and Simulated Annealing," *IEEE Transactions on Pattern Analysis and Machine Intelligence*, vol. 16, pp. 976–986, 1994.
- [43] M. Leventon, W. Grimson, and O. Faugeras, "Statistical Shape Influence in Geodesic Active Contours," *IEEE Transactions on Computer Vision and Pattern Recognition*, vol. 1, pp. 316–323, 2000.
- [44] L. Ding, A. Goshtasby, and M. Satter, "Volume Image Registration by Template Matching," *Image and Vision Computing*, vol. 19, no. 12, pp. 821–832, October 2001.
- [45] A. Goshtasby, "Image Registration by Local Approximation Methods," *Image and Vision Computing*, vol. 6, no. 4, pp. 255–261, November 1988.
- [46] C. K. I. Williams, M. Revow, and G. E. Hinton, "Instantiating Deformable Models with a Neural Net," *Computer Vision and Image Understanding*, vol. 68, no. 1, pp. 120–126, October 1997.
- [47] A. Goshtasby, S. H. Gage, and J. F. Bartholic, "A Two-Stage Cross-Correlation Approach to Template Matching," *IEEE Transactions on Pattern Analysis and Machine Intelligence*, vol. 6, no. 3, pp. 374–378, 1984.
- [48] J. P. Lewis, "Fast Template Matching," *Vision Interface*, pp. 120–123, 1995.
- [49] J. Lewis, "Fast Normalized Cross-Correlation," in *Vision Interface*. Canadian Image Processing and Pattern Recognition Society, 1995, pp. 120–123.

- [50] R. C. Gonzalez and P. Wintz, *Digital Image Processing (3rd Edition)*, R. Woods, Ed. Reading, Massachusetts: Addison-Wesley, 1992.
- [51] D. I. Barnea and H. F. Silverman, “A Class of Algorithms for Fast Digital Image Registration,” *IEEE Transactions on Computers*, vol. 21, pp. 179–186, 1972.
- [52] G. Borgefors, “Hierarchical Chamfer Matching: A Parametric Edge Matching Algorithm,” *IEEE Transactions on Pattern Analysis and Machine Intelligence*, vol. 10, no. 6, pp. 849–865, November 1988.
- [53] H. G. Barrow, J. M. Tenenbaum, R. C. Bolles, and H. C. Wolf, “Parametric Correspondence and Chamfer Matching: Two New Techniques for Image Matching,” *Proceedings of the Fifth International Joint Conference on Artificial Intelligence*, pp. 659–663, 1977.
- [54] M. Ulrich, C. Steger, and A. Baumgartner, “Real-Time Object Recognition Using a Modified Generalized Hough Transform,” *Pattern Recognition*, vol. 36, pp. 2557–2570, 2003.
- [55] J. Canny, “A Computational Approach to Edge Detection,” *IEEE Transactions on Pattern Analysis and Machine Intelligence*, vol. 8, no. 6, pp. 679–698, 1986.
- [56] R. C. Eberhart, J. Kennedy, and Y. H. Shi., *Swarm Intelligence*. USA: Kauffman Publishers, 2001.
- [57] J. Kennedy and R. C. Eberhart, “Particle Swarm Optimization,” *IEEE International Conference on Neural Networks*, vol. 1, no. 1, 1995.
- [58] J. Spiller and T. Marwala, “Evolutionary Algorithms for Warp Control Point Placement,” March 2007, submitted to The 2nd International Symposium on Intelligence Computation and Applications.
- [59] L. Zagorchev and A. Goshtasby, “A Comparative Study of Transformation Functions for Nonrigid Image Registration.” *IEEE Transactions on Image Processing*, vol. 15, no. 3, pp. 529–538, March 2006.
- [60] T. J. Rivlin, *An Introduction to the Approximation of Functions*. Waltham, MA, USA: Blaisdell Publishing Co, 1969.

- [61] H. F. Davis, *Fourier Series and Orthogonal Functions*. USA: Allyn and Bacon, 1966.
- [62] G. E. Forsythe, "Generation and Use of Orthogonal Polynomials for Data Fitting with a Digital Computer," *Journal of the Society of Industrial Applied Mathematics*, vol. 5, no. 2, pp. 74–88, 1957.
- [63] D. H. McLain, *Mathematical Methods in Computer Graphics Design*, 1980, ch. Interpolation Methods for Erroneous Data, pp. 87–104.
- [64] D. Shepard, "A Two-Dimensional Interpolation Function for Irregularly Spaced Data," *Proceedings of the 23rd National Conference. ACM*, pp. 517–524, 1968.
- [65] I. K. Crain and B. K. Bhattacharyya, "Treatment of Non-Equispaced Two-Dimensional Data with a Digital Computer," *Geoexploration*, vol. 5, pp. 173–194, 1967.
- [66] A. D. Maude, "Interpolation for Graph Plotters," *Journal of Computers*, vol. 16, pp. 64–65, 1973.
- [67] Y. Zhong, A. K. Jain, and M. P. Dubuisson-Jolly, "Object Tracking Using Deformable Templates," *IEEE Transactions on Pattern Analysis and Machine Intelligence*, vol. 22, no. 5, pp. 544–549, MAY 2000.

## Chapter 2

# Evolutionary Algorithms for Warp Control Point Placement

This paper has been submitted to *The 2nd International Symposium on Intelligence Computation and Applications*, to take place in Wuhan, China, during September 2007. Accepted papers are to be published by Springer in LNCS. This paper deals with the warp methodology of the localization algorithm, and presents a comparative analysis of the evolutionary optimization methods tested for warp control point placement.

# Evolutionary Algorithms for Warp Control Point Placement

Jonathan Spiller and Tshilidzi Marwala

School of Electrical and Information Engineering,  
University of the Witwatersrand,  
Johannesburg, South Africa  
{j.spiller,t.marwala}@ee.wits.ac.za  
<http://www.wits.ac.za>

**Abstract.** Object localization requires the deformation and registration of templates with a target image. A warping and registration methodology is presented to facilitate this task, utilizing evolutionary optimization routines to automatically determine optimal control point placement between template and target image. The Local Weighted Mean warp used to deform the templates to fit these control points is presented, along with a discussion of three evolutionary algorithms and their application to the problem. The optimization routines of Genetic Algorithm, Particle Swarm Optimization and Simulated Annealing are compared in terms of accuracy, speed and computational requirements, with Particle Swarm Optimization being highlighted as the best method for this task.

**Key words:** Template Warping, Registration, Genetic Algorithm, Particle Swarm Optimization, Simulated Annealing.

## 1 Introduction

Prototype-based localization schemes typically require the warping of templates and their registration with a target image [1]. A general localization scheme of this type has been developed, that uses a multistage, multiresolution algorithm to facilitate a computationally efficient search. The initial stages of the algorithm are tasked with reducing the search space and determining approximate template matches, while the final stage involves warping of the template to fit salient image features. A novel template warping and registration method, using evolutionary algorithms to determine optimal control point placement for template warping, has been developed specifically for this object localization algorithm. The aim of this research is to determine which of the evolutionary algorithms is best suited for use in the final algorithm implementation.

This paper presents the warp methodology of the localization algorithm, along with a comparison of the three evolutionary optimization techniques tested for the determination of control point locations. These are:

- Genetic Algorithm (GA).

- Particle Swarm Optimization (PSO).
- Simulated Annealing (SA).

The template deformation method presented is adaptable to a wide variety of warping and registration tasks [2], and the algorithm has already been successfully applied to medical image segmentation [3], target recognition from aerial images, text recognition, as well as general object localization tasks [2]. A comprehensive review of the full localization algorithm is beyond the scope of this paper, but can be found in [2].

The rest of this paper is set out as follows: Section 2 gives a brief overview of the registration problem, briefly discussing the algorithm and the registration requirements. Section 3 describes the warp methodology, detailing the Local Weighted Mean warp. The three evolutionary algorithms are detailed in Section 4. The results of a number of warp tests, as well as a comparison of the performances of the three algorithms, are given in Section 5.

## 2 Registration for Object Localization

Typical registration problems involve the overlaying of two images of the same scene, and require the determination of a set of corresponding control point positions on the two images [4]. Once a correspondence between these control points has been established, they are used to determine a transformation function that maps the rest of the points in the image. Control point selection can be accomplished either manually or automatically. Manual selection may require high level, expert knowledge, while automatic methods typically rely on line intersections, locally maximum variances and curvatures or centers of gravity as control point positions. Control point placement for the warp used in this algorithm relies on a different approach.

Although control points are manually selected on the template image, the sub-sampled target image is unknown before localization and the required corresponding control point locations on this image can therefore not be defined. However, the localization algorithm for which this method was developed does align the template and target image to some extent. This fact is used to infer the required control point locations from the template, by overlaying the template and localized target images. A discussion of the localization algorithm is beyond the scope of this paper, but it is detailed extensively in [2].

With the template overlaying the sub-sampled target image (as a result of the previous stages of the localization algorithm), the control point locations on the template are used to approximate sets of corresponding control points on the target edge map. The evolutionary methods of GA, PSO and SA are then used to shift the control points within each set before the template is warped to fit the new points. This warp facilitates the registration between the deformed template and the target image. The accuracy of the registration is determined by measuring the energy between the now deformed template and the sub-sampled

target edges using the cost function [5]:

$$E = \frac{1}{N_T} \sum_{i=1}^{N_T} \{1 + \Phi_i(x, y) |\cos [\beta(x, y)]|\} \quad (1)$$

Where  $\Phi_i(x, y)$  is the edge potential (see [5]) of pixel  $i$  and the summation covers the  $N_T$  pixels on the template.  $\beta(x, y)$  is the angle between the tangent of the target edge pixel *nearest*  $(x, y)$  and the tangent direction of the template at  $(x, y)$ .

### 3 Template Warping

Inference of the appropriate transformation function is crucial to the accuracy of registration. Global transformations are typically used to register images that do not contain local geometric distortion [4]; however, template registration may require local geometric distortion depending on the local structure of the scene. The locally sensitive transformation function used for template warping in this algorithm is described here.

Given  $N$  corresponding control points  $(X_i, Y_i)$  on the template and  $(x_i, y_i)$  on the sub-sampled target image, the LWM warp requires two functions,  $X_i \approx f(x_i, y_i)$  and  $Y_i \approx g(x_i, y_i)$ , that approximate a mapping between these points as accurately as possible [4]. The problem is reformulated to give two sets of  $N$  3D points,  $(x_i, y_i, X_i)$  and  $(x_i, y_i, Y_i)$ , requiring the determination of the functions  $f$  and  $g$  [4]. The determination of the function  $f$  only is described here, since the function  $g$  can be determined in the same manner.  $f$  is typically taken to be a polynomial of order  $T$ , of the form [4, 6]:

$$f(x, y) = \sum_{j=0}^T a_j P_j(x, y) . \quad (2)$$

The set of  $T$  polynomials  $P_j(x, y)$  are constructed by the Gramm-Schmidt orthogonalization process, using a set of linearly independent functions  $h_i(x, y)$ , to have the form [7]:

$$P_T(x, y) = a_{T0}P_0(x, y) + a_{T1}P_1(x, y) + \dots + a_{TT}h_T(x, y) . \quad (3)$$

A problem with using the transformation function of (2), is that local geometric differences, as well as local control point inaccuracies, are averaged out equally over the whole image [4]. The effect of geometric difference and/or measurement inaccuracy is the same irrespective of how near or far the control point is to the approximating point. This is a highly undesirable property for a template warp that requires local geometric distortion to achieve the required deformation. To localize the transformation, a weight function is defined that represents the influence of each  $i^{th}$  control on a point  $(x, y)$  by the inverse Euclidean distance between them. The weight function ensures a strictly local geometric warp

that is influenced only by the appropriate control point  $(x_i, y_i, X_i)$ , and  $n - 1$  of its nearest neighbors. The weight function is given by [4]:

$$\begin{cases} W_i(R) = 1 - 3R^2 + 2R^3 & 0 \leq R \leq 1. \\ W_i(R) = 0 & R \geq 1. \end{cases} \quad (4)$$

Where:  $R = [\delta + (x - x_i)^2 + (y - y_i)^2]^{\frac{1}{2}}/R_n$  and  $R_n$  is the distance of point  $(x_i, y_i)$  from its  $(n - 1)^{th}$  nearest control point in the target image.  $\delta$  defines the influence of control points on the approximating point. The smaller the value of  $\delta$  the smaller the influence of distant control points, allowing a more local warp. Large values of  $\delta$  decrease the influence of nearby control points, allowing for a smoother warp.  $\delta$  also prevents the weight function from becoming infinite where  $x = x_i$  and  $y = y_i$ . The form of the weighting function guarantees that polynomial  $i$  has no influence on points whose distance from control point  $(x_i, y_i)$  is larger than  $R_n$ . The weighted sum of the polynomials is continuous and smooth at all values of  $(x, y)$ , since [4]:  $[\frac{dW}{dR}]_{R=0} = [\frac{dW}{dR}]_{R=1} = 0$ .

As can be seen, different weights  $W_i(x, y)$  are obtained for different points  $(x, y)$  and can therefore be considered as a function of the position of points in the target image. By incorporating the weighting factor into the set of polynomials of equation 3, the parameters can be shown to be given by [8]:

$$a_{jk}(x, y) = -a_{jj}(x, y) \frac{\sum_{i=1}^N W_i(x, y) P_k(x_i, y_i) h_j(x_i, y_i)}{\sum_{i=1}^N W_i(x, y) [P_k(x_i, y_i)]^2}. \quad (5)$$

$$j = 1, \dots, T; \quad k = 1, \dots, T - 1.$$

Since the approximating transformation is still defined by equation (2), the coefficients  $a_j$  can be found using [4]:

$$a_j(x, y) = \frac{\sum_{i=1}^N W_i(x, y) X_i P_j(x_i, y_i)}{\sum_{i=1}^N [W_i(x, y) P_j(x_i, y_i)]^2}. \quad (6)$$

This yields the final transformation function which defines the  $X$  value (in the template) of an arbitrary point  $(x, y)$  (in the target image) by the weighted sum of polynomials having a non-zero weight over that point. The Local Weighted Mean function is given by [4, 9]:

$$f(x, y) = \frac{\sum_{i=1}^N W \left\{ [\delta + (x - x_i)^2 + (y - y_i)^2]^{\frac{1}{2}}/R_n \right\} P_i(x, y)}{\sum_{i=1}^N W \left\{ [\delta + (x - x_i)^2 + (y - y_i)^2]^{\frac{1}{2}}/R_n \right\}}. \quad (7)$$

Where  $P_i(x, y)$  is the polynomial passing through point  $(x_i, y_i, X_i)$  and  $n - 1$  other points nearest to it.

## 4 Evolutionary Algorithms

Evolutionary optimization techniques exploit randomness to obtain optimal solutions to a problem[10]. Being heuristic, they are not mathematically guaranteed

to converge, but instead are designed to search a large space and find a number of good solutions [10]. Various evolutionary methods are used to control and manipulate a population of possible solutions in order to explore a global search space. In this application however, the localization algorithm of [2] aligns the template and target images before warping, so the optimization inherently takes place within the region of the global minimum. The search space for the problem is therefore modified so that the optimization routines perform a comprehensive search within the *region* of the global minimum, as opposed to the usual global search over the entire search space.

The first step in all the evolutionary algorithms is the initialization of the population. This is achieved by “tracing” the set of control points from the template onto the sub-sampled target image and then shifting the points slightly to obtain a population of different sets. Each control point is shifted with sub-pixel accuracy to a new position within the local neighborhood of the original control point. The population is generated to have a normal distribution across the search space in order to cover a wide spectrum of possible solutions. The normal distribution ensures a mix of both good and diverse solutions in order to maximize the chance of locating the global or optimum solution [11]. Once initialization is complete, the algorithms begin to evolve the population.

The three evolutionary techniques tested for template registration are described in this section.

#### 4.1 Genetic Algorithm

Genetic Algorithm (GA) was introduced by John Holland in 1975 and has been defined as a stochastic algorithm whose search method tries to model the biological phenomena of genetic inheritance and natural selection [12]. The basic concept of GA is to simulate processes in natural systems necessary for evolution [10], specifically those that follow the principles first laid down by Charles Darwin, of survival of the fittest. As such they represent an intelligent exploitation of a random search within a defined search space to solve a problem.

Like most evolutionary methods, GA operation is based on a population of individuals that represent a number of possible solutions to the problem. The population is evolved over a number of iterations in order to optimize a given problem solution. Terminology is taken directly from genetic theory, with each individual (solution) possessing a number of chromosomes (variables), which in turn are made up from a number of genes (bits or real numbers). Evolution of the population at each iteration is accomplished through the use of evolutionary operators that model natural evolutionary phenomena. The selection operator is used to determine which individuals in a population are selected to produce offspring [12]. Crossover models the process of reproduction, and involves the selection of a point or points in two parent individuals and the exchange of genes between these individuals about the selected point/s [10]. Mutation is implemented in GA to maintain diversity within the population and ensure that the largest possible search space is explored [10].

## 4.2 Particle Swarm Optimization

Particle Swarm Optimization (PSO) was developed in 1995 by Dr Russel Eberhart and Dr James Kennedy [13]. It is a stochastic, population-based technique, inspired by the social behavior of flocking birds and schooling fish [13]. As with GA, the system is initialized with a population of solutions and searches for optima by updating generations. However, unlike GA, PSO has no evolutionary operators such as crossover and mutation.

In PSO, each potential solution is represented by a particle. Particles fly through the problem space by following the current optimum particle [14]. During flight, each particle adjusts its position according to its own experience, and according to the experience of its neighboring particles, making use of the best position encountered by itself and its neighbors. In this way, the whole swarm contributes to the solution of the problem [14].

Each particle in the swarm is initialized in the same manner as the GA individuals, and with a semi-random velocity. During each iteration of the algorithm, each particle's velocity and position is updated according to Equations 8 and 9 respectively. The fitness of each particle is evaluated through the system's cost function, and the best fitness, along with its corresponding position, is stored for each particle. It can be seen that Equation 8 comprizes three terms. The first term is a portion of current motion, the second term is an influence of the current particle memory, while the third term is an influence of the swarm memory [15].

$$v_{k+1}^i = wv_k^i + c_1rand(p^i - x_k^i) + c_2rand(p_k^g - x_k^i). \quad (8)$$

Where:

$v_i$ – Velocity of $i^{th}$ particle.	$k$ – Iteration number.
$w$ – Particle inertial factor.	$p^i$ – Best position of $i^{th}$ particle.
$x^i$ – Position of $i^{th}$ particle.	$p^g$ – Best position of <b>any</b> particle.
$c_1$ – Cognitive scaling factor.	$c_2$ – Social scaling factor.

$$x_{k+1}^i = x_k^i + v_{k+1}^i. \quad (9)$$

Where:

$x^i$ – Position of $i^{th}$ particle.	$v^i$ – Velocity of $i^{th}$ particle.
$k$ – Iteration number.	

## 4.3 Simulated Annealing

Simulated Annealing (SA) is an optimization technique based on the physical process of annealing. It exploits an analogy between the energy of a cooling metal and the cost function of a combinatorial optimization problem [16]. The algorithm is based upon the Metropolis method, and was originally proposed as a means of finding the equilibrium configuration of a collection of atoms at a given temperature [17]. The adaptation of this algorithm to the domain of mathematical optimization for combinatorial functions was pioneered by S. Kirkpatrick, C. Gelatt and M. Vecchi in 1983 [16].

In the SA algorithm, a starting temperature  $T_s$  is selected and a single solution  $X_i$  is generated (in the same manner as for GA and PSO) to represent an energy state. The cost function of the system is used to evaluate the the energy of  $X_i$ . A new energy state is then generated at random and its energy is also calculated. If the new state has a lower energy than the previous one, then it is accepted as the new solution, thus decreasing the cost function. If the energy of the new state is higher than the previous one, it still has a probability to be accepted, given by Equation 10.

$$P = \exp\left(-\frac{E(X_{i+1}) - E(X_i)}{T}\right). \quad (10)$$

Where:

$E(X)$  – Energy of State  $X$ .       $T$  – Current Temperature.

This probability allows the algorithm to accept states of higher energy than the current state, and gives SA the ability to avoid becoming trapped within local minima [16]. As the algorithm proceeds, the temperature  $T$  decreases with each iteration according to a cooling schedule. With a decreasing  $T$ , the probability of accepting higher energy states decreases, forcing the algorithm to refine its search for the global minimum. The SA algorithm terminates when  $T$  reaches a specified  $T_{min}$ .

## 5 Results

The optimization routines were applied to three different warps, with each routine being evaluated in terms of warp accuracy, time requirements and general computational expense. Table 1 shows a comparison of the accuracies achieved by each routine, the time taken to run 100 iterations, and the number of function evaluations required by each routine. An evaluation of the number of function evaluations compared to time taken gives an indication of computational requirements. A large number of evaluations in a short space of time indicates a resource-intensive algorithm, while a large number of evaluations in a long time frame indicates high computational expense. Results are given for the three different warps, which are also illustrated graphically. These results were then aver-

**Table 1.** Comparison of Optimization Routines Applied to Three Warps.

	Hand			Fish			Owl		
	Error	Time (s)	Fn Evals	Error	Time (s)	Fn Evals	Error	Time (s)	Fn Evals
GA	0.071	6.14	1404	0.136	8.01	2207	0.101	7.24	1568
PSO	0.066	2.97	652	0.102	3.79	928	0.086	3.40	775
SA	0.109	28.60	25912	0.188	36.24	38133	0.167	32.95	30962

aged over the three warps to obtain a mean result for each optimization routine.

The mean performance measure is depicted graphically in Fig. 1, which illustrates the convergence characteristics of each routine. This performance measure is useful in that it gives an indication of the general capabilities of each method under typical operational conditions.

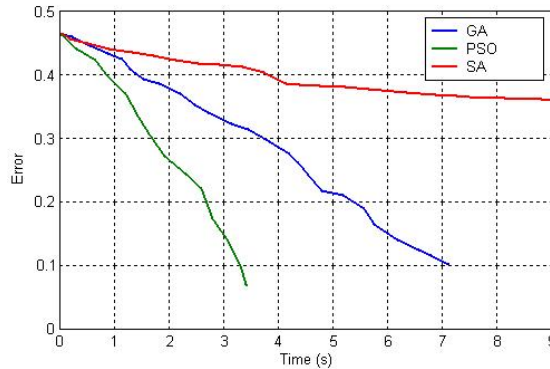


**Fig. 1.** Average convergence characteristics of GA, PSO and SA.



**Fig. 2.** Hand warp using GA: Image sequence showing initial to final template warps at 15 iteration intervals.

**Genetic Algorithm.** The GA uses its population to good effect to explore the search space, resulting in an average energy of  $E = 0.102$ . It takes approximately twice as long as the PSO to perform 100 iterations. This is due to the disruptive nature of selection, crossover and mutation, as well as the distributed nature of the search. However, the distributed nature of the algorithm also makes it extremely robust, allowing it to quickly explore the entire search space.

**Particle Swarm Optimizaion.** The PSO algorithm proved to be the best of the evolutionary methods. On average, it reaches a solution twice as fast as the GA and with a slightly better average energy of  $E = 0.084$ . The algorithm proved to be extremely robust, converging quickly and to a high accuracy for all test cases. The speed of the algorithm is attributed to the simplicity of computation

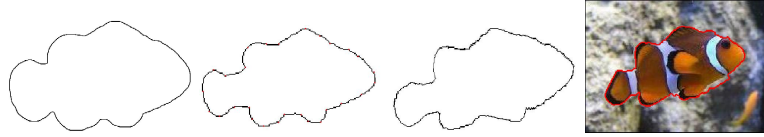


**Fig. 3.** Fish warp using SA: Template warps at 0, 50, 75 iterations and final template localization.

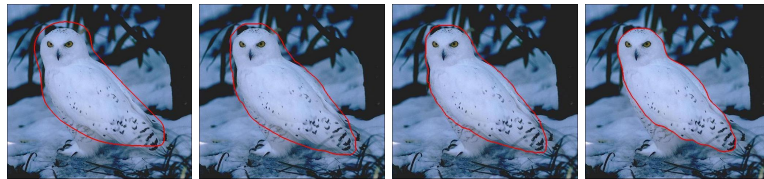


**Fig. 4.** Owl warp using PSO: Image sequence shows actual implementation of the localization algorithm at 0, 20, 50 and 100 iterations.

and to the decreasing of the particles' inertia of with progressive iterations. As with the GA, the PSO is well suited to exploration of the entire search space.

**Simulated Annealing.** The SA algorithm proved to be the poorest of the tested algorithms. An average error of  $E = 0.154$  was obtained; however, this was achieved in a prohibitively long time. The SA required approximately 30s to converge to an accurate solution. This is attributed to the highly random generation of successive energy states, and may also in part be due to a non-optimal cooling schedule and temperature scale.

## 6 Conclusion

A warping and registration method has been presented for the deformation of templates in a target localization scheme. Variational template warps are generated based on the arrangement of control points on the prototype template, by utilizing evolutionary algorithms to shift these points to new locations. A Local Weighted Mean template warping methodology was presented for the warping, along with a brief explanation of the use of Genetic Algorithm, Particle Swarm Optimization and Simulated Annealing for this application. The evolutionary routines were tested for control point determination and compared in terms of accuracy, speed and computational requirements. PSO was found to yield the highest accuracy in the shortest time while also achieving the best computational efficiency of the three methods. It is therefore proposed to use PSO to facilitate warping in the localization scheme.

## References

1. U. Grenander, "Pattern Synthesis: Lectures in Pattern Theory," *Applied Mathematical Sciences*, vol. 18, Springer-Verlag, 1976.
2. J. M. Spiller, "Object Localisation Using Deformable Templates," Master's thesis, School of Electrical and Information Engineering, University of the Witwatersrand, Johannesburg, South Africa, April 2007.
3. J. M. Spiller and T. Marwala, "Medical Image Segmentation and Localization Using Deformable Templates," in *Proceedings of the International Federation of Medical and Biological Engineering*, E. S. I. Kim and T. S. Sah, Eds., vol. 14. Springer-Verlag, Berlin Heidelberg, 2006, pp. 2176–2179.
4. A. Goshtasby, "Image Registration by Local Approximation Methods," *Image and Vision Computing*, vol. 6, no. 4, pp. 255–261, November 1988.
5. A. K. Jain, Y. Zhong, and S. Lakshmanan, "Object Matching Using Deformable Templates," *IEEE Transactions on Pattern Analysis and Machine Intelligence*, vol. 18, no. 3, pp. 267–278, MARCH 1996.
6. L. Zagorchev and A. Goshtasby, "A Comparative Study of Transformation Functions for Nonrigid Image Registration." *IEEE Transactions on Image Processing*, vol. 15, no. 3, pp. 529–538, March 2006.
7. H. F. Davis, *Fourier Series and Orthogonal Functions*. USA: Allyn and Bacon, 1966.
8. G. E. Forsythe, "Generation and Use of Orthogonal Polynomials for Data Fitting with a Digital Computer," *Journal of the Society of Industrial Applied Mathematics*, vol. 5, no. 2, pp. 74–88, 1957.
9. A. D. Maude, "Interpolation for Graph Plotters," *Journal of Computers*, vol. 16, pp. 64–65, 1973.
10. M. Gen and R. Cheng, *Genetic Algorithms and Engineering Design*. New York: John Wiley and Sons, 1997.
11. B. Bhanu, L. Sungkee, and S. Das, "Adaptive Image Segmentation Using Genetic and Hybrid Search Methods," *IEEE Transactions on Aerospace and Electronic Systems*, vol. 31, no. 4, pp. 1268–1291, October 1995.
12. K. T. Ko, K. S. Tang, C. Y. Chan, K. F. Man, and S. Kwong, "Using Genetic Algorithms to Design Mesh Networks," *Computer*, vol. 30, no. 8, pp. 56–61, 1997.
13. J. Kennedy and R. Eberhart, "Particle Swarm Optimization," *Proceeding of the IEEE International Conference on Neural Networks*, vol. 1, no. 1, pp. 1942–1948, 1995.
14. D. Boeringer and D. H. Werner, "A Comparison of Particle Swarm Optimization and Genetic Algorithms for a Phased Array Synthesis Problem," *Antennas and Propagation Society International Symposium*, vol. 1, pp. 181–184, June 2003.
15. K. E. Parsopoulos and M. N. Vrahatis, "Particle Swarm Optimization Method in Multiobjective Problems," in *SAC '02: Proceedings of the 2002 ACM Symposium on Applied Computing*. New York, NY, USA: ACM Press, 2002, pp. 603–607.
16. S. Kirkpatrick, C. D. Gelatt, and M. P. Vecchi, "Optimization by Simulated Annealing," *Science*, vol. 220, no. 4598, pp. 671–680, 1983.
17. R. Salazar and R. Toral, "Simulated Annealing Using Hybrid Monte Carlo," *Journal of Statistical Physics*, vol. 89, pp. 1047–1060, 1997.

## Chapter 3

# Medical Image Segmentation and Localization Using Deformable Templates

This paper was presented at the *World Congress on Medical Physics and Biomedical Engineering* in Seoul, Korea, in 2006. It presents a specific application of the localization algorithm to functional medical images.

# Medical Image Segmentation and Localization using Deformable Templates

J.M.Spiller<sup>1</sup>, T. Marwala<sup>1</sup>

<sup>1</sup> School of Electrical & Information Engineering, University of the Witwatersrand, Johannesburg, South Africa

**Abstract**— This paper presents deformable templates as a tool for segmentation and localization of biological structures in medical images. Structures are represented by a prototype template, combined with a parametric warp mapping used to deform the original shape. The localization procedure is achieved using a multi-stage, multi-resolution algorithm designed to reduce computational complexity and time. The algorithm initially identifies regions in the image most likely to contain the desired objects and then examines these regions at progressively increasing resolutions. The final stage of the algorithm involves warping the prototype template to match the localized objects. The algorithm is presented along with the results of four example applications using MRI, x-ray and ultrasound images.

**Keywords**— Deformable template, Localization, Segmentation, Multi-resolution algorithm, Medical imaging.

## I. INTRODUCTION

Image segmentation and localization plays an important role in many medical imaging applications by automating or facilitating the delineation of anatomical structures. Since all subsequent interpretation tasks, such as feature extraction, object recognition, and classification depend largely on the quality of the segmented output, effective segmentation has become a critical step for automated analysis in medical imaging. Segmentation and localization of anatomical structures is difficult in practice, especially when dealing with inherently noisy, low spatial resolution images such as those produced using functional imaging.

Deformable Templates provide a powerful tool for image segmentation, by exploiting constraints derived from the image data together with *a priori* knowledge about the location, size, and shape of the required structures [1].

The algorithm presented here is used to find a match between a deformed template and objects in the image, by minimizing a cost function between the template and object boundary. The algorithm achieves computational efficiency by searching the image in a number of stages and resolutions, refining the search at each stage. Object Localization requires that the template be matched regardless of the object's displacement, rotation, scale and deformation. Invariance to these characteristics is incorporated at each stage of the algorithm using discrete template orientations.

## II. A MODEL OF DEFORMATION

The model of deformation presented is based on the pattern theoretic model of Grenander [2]. It consists of two parts:

1. A prototype template image  $T_0$  describing the overall architecture of the shape in terms of its representative contours and edges.
2. A set of control points (CPs) on the template, used to define a parametric mapping governing the deformation of the prototype.

The prototype template is based on average or expected image evidence and is designed to capture expert, prior knowledge of the shape, size and orientation of the anatomical structure to be localized.

The CPs are defined on the image before the localization process commences and are used to facilitate warping of the prototype to create shape variation. These points can be placed to incorporate expert knowledge of where shape variation is more likely to occur.

This type of model is particularly appropriate in medical image segmentation, where inexact knowledge about the shape of an object is available and where it is necessary to accommodate the often significant variability of biological structures over time and across different individuals [3]. Figure 1 shows a typical template and base image.

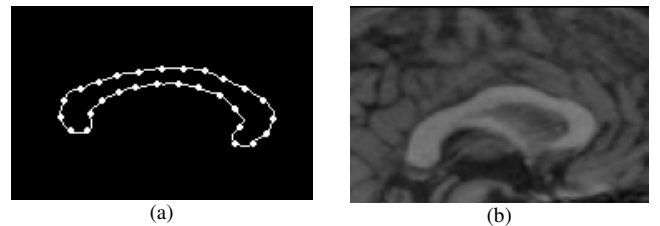


Fig. 1. Deformable Template Matching: (a) A prototype template of a typical Corpus Callosum shape with control points. (b) MRI base image where the Corpus Callosum must be localized and segmented.

## III. THE MULTI-STAGE ALGORITHM

In typical applications, an object has to be locatable regardless of translation, rotation and size. Given that the

localization also needs to be invariant to partial shape changes, this introduces a large number of variables to be determined during optimization. Objective functions are typically non-convex, and so a multi-stage algorithm is employed to reduce the search space [1]. Using the algorithm described in this section, objects' localization and segmentation is accomplished in 10s-30s.

*Stage 1 – Regions of Interest:* This stage is designed to reduce the search space by identifying the correct regions of the image to search for an object.

The template  $T$  with dimensions  $X$  and  $Y$  is convolved with the edges of the base image  $B$  using a 2D convolution filter in the spatial domain [4].

$$C(X, Y) = \sum_{x=1}^{\text{size}(X)} \sum_{y=1}^{\text{size}(Y)} T(x, y)B(X - x, Y - y) \quad (1)$$

The result of the convolution is given by Equation 1 and represents the image as an intensity map with high intensity where the convolution integral is large.

Template-sized regions of high intensity are searched for object matches in the next stage of the algorithm. Using only these areas, the visual search space can be reduced by up to 80%.

*Stage 2 – Multi-Resolution Approximate Matches:* During this stage, possible object matches are determined using approximate matching.

The template is windowed at discrete positions and orientations over the base image, and a match between the two is evaluated. The discrete window locations do not cover the entire base image, but are obtained from Stage 1.

The template is attracted and aligned to the salient edges in the base image via directional Edge Potential Fields (EPFs), determined by the positions and directions of edges in the base image [1]. The EP for each pixel in the base image is defined by:

$$\Phi(x, y) = -\exp\left(-\sqrt{(\delta_x^2 + \delta_y^2)}\right) \quad (2)$$

Where  $(\delta_x, \delta_y)$  is the displacement from the pixel to the nearest edge point in the image. A directional component is also included for each pixel  $(x, y)$  in edge  $I$ , determined by:

$$\Theta(x, y) = \arctan\left(\frac{dI(x, y)}{dy} \Big/ \frac{dI(x, y)}{dx}\right) \quad (3)$$

This modified EPF induces an energy function between the template image and the base image given by [1]:

$$E(T_{s, \theta, \zeta, d}, B) = \frac{1}{N_T} \sum_{i=1}^{N_T} (1 + \Phi_i(x, y) |\cos(\beta(x, y))|) \quad (4)$$

Where the summation is over the  $N_T$  pixels on the template, and  $\beta(x, y)$  is the angle between the tangent of the base edge pixel *nearest*  $(x, y)$  and the tangent direction of the template *at*  $(x, y)$ . This energy measure, expressed as a correlation between the base image and the template deformed in terms of scale  $s$ , rotation  $\theta$ , displacement  $d$  and warp  $\zeta$ , is based on the Chamfer matching function but requires that the template agree with the image edges not only in position, but also in direction [1]. This requirement provides significantly improved robustness in noisy images. The locations of low energy matches (below an application-specific threshold) are taken as possible matches.

The resolution of the EPF image is controlled by varying the standard deviation  $\sigma$ , of the Gaussian filter used to find the image edges [5]. Once the set of possible matches is found at a coarse resolution, Stage 2 is repeated at progressively finer resolutions to determine final matches. The locations of possible matches at previous resolutions are used as starting locations for finer resolution matching.

*Stage 3 – Template Deformation:* At this stage, the template is deformed to fit the image edges accurately. This deformation can be thought of as a registration between the template image and the base.

The approximate match locations from the finest resolution EPFs are used to initialize the template placement on the base edge-map. Control points on the template are transferred to corresponding locations on the edge-map and are then repositioned iteratively using Particle Swarm optimization (PSO) [6]. At each iteration of the PSO algorithm, a Local Weighted Mean (LWM) warp [7] is used to deform the template to fit these new CP positions. The PSO algorithm can be run for a specified number of iterations, or until a terminating criterion, such as a minimum energy, is met.

Given  $N$  corresponding CPs  $(X_i, Y_i)$  on the template and  $(x_i, y_i)$  on the base image, LWM warping requires two functions,  $X_i \approx f(x_i, y_i)$  and  $Y_i \approx g(x_i, y_i)$ , that approximate a mapping between these points, as closely as possible. The transformation functions can be obtained directly from the given control points and do not require the solution of systems of equations.  $f$  (and similarly  $g$ ) are obtained from Equation 5 [7].

$$f(x, y) = \frac{\sum_{i=1}^N W \{ [(x - x_i)^2 + (y - y_i)^2]^{1/2} / R_n \} P_i(x, y)}{\sum_{i=1}^N W \{ [(x - x_i)^2 + (y - y_i)^2]^{1/2} / R_n \}} \quad (5)$$

Where the  $N$  polynomials  $P_i$  are constructed by the Gram-Schmidt orthogonalization process, using a set of linearly independent functions  $h_i$ , to have the form [7]:

$$\begin{aligned}
P_0(x, y) &= a_{00}h_0(x, y) \\
P_1(x, y) &= a_{10}P_0(x, y) + a_{11}h_1(x, y) \\
P_2(x, y) &= a_{20}P_0(x, y) + a_{21}P_1(x, y) + a_{22}h_2(x, y) \\
&\vdots \\
P_T(x, y) &= a_{T0}P_0(x, y) + a_{T1}P_1(x, y) + \dots + a_{TT}h_T(x, y)
\end{aligned} \tag{6}$$

Where  $(x, y)$  is any arbitrary point in the image. The  $N$  weight functions  $W_i$  are given by:

$$\begin{aligned}
W_i(R) &= 1 - 3R^2 + 2R^3 & 0 \leq R \leq 1 \\
W_i(R) &= 0 & R > 1
\end{aligned} \tag{7}$$

Where  $R = [(x - x_i)^2 + (y - y_i)^2]^{\frac{1}{2}} / R_n$  and  $R_n$  is the distance of point  $(x_i, y_i)$  from its  $(n-1)^{\text{th}}$  nearest control point in the base image.

Apart from not requiring the solution of a system of equations at each iteration, this LWM warp implementation has a number of other advantages over alternate warp methods [8]:

- Corresponding control points are not mapped exactly to each other so digital errors in the correspondences as well as small mismatch errors are smoothed.
- The rational weight functions adapt to the density and organization of the points and automatically extend to large gaps between control points.
- Because varied placement of control points is acceptable, expert knowledge of deformation can be incorporated.

The use of PSO to determine the optimal placement of CPs is effective because the regions of the global minima are known from Stage 2. To prevent the PSO from exploring outside of these regions, and to limit warp dimensionality, a penalty function is introduced that measures the sum of the squared differences between CPs on the original and deformed templates. The penalty function is added to the energy cost given in Equation 4 and penalizes extreme warps that would leave the region of the global minimum. It is given by Equation 8, where  $\alpha$  controls rigidity of the warp.

$$P(x, y) = \alpha \sum_{x=1}^N (X_i - x_i)^2 + (Y_i - y_i)^2 \tag{8}$$

#### IV. EXPERIMENTAL RESULTS

The deformable template model presented has been applied to different biological structures in a number of functional medical images. All images were obtained from the Tagare Medical Image Database [9].

The first test experiment presented involves the segmentation of the Corpus Callosum in four different MRI images. The prototype template used is the first Corpus Callosum shape. This experiment is intended to illustrate the warp capabilities of the algorithm, and the template image is initialized at the center of the base images. Figure 2 shows the initial and final base images. As can be seen, all four Corpus Callosus are localized and segmented, even though there is considerable shape variation between the images.

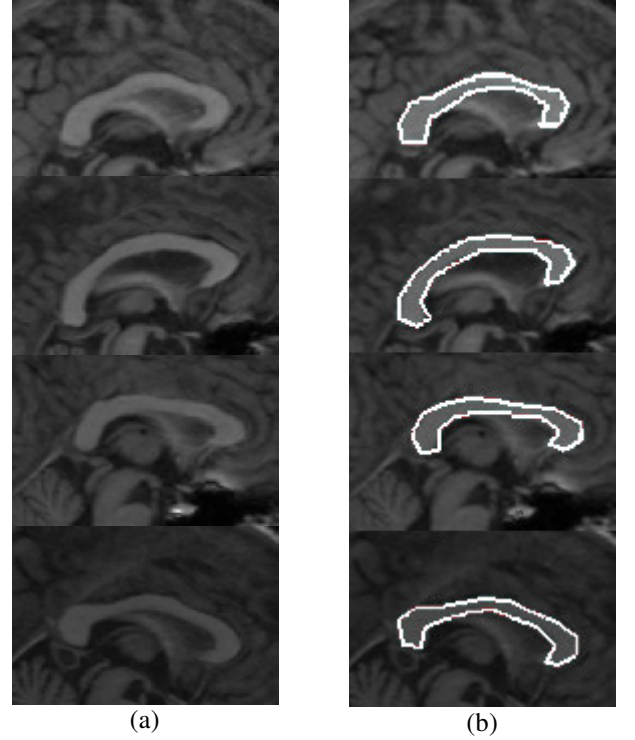


Fig. 2. Corpus Callosum MRI images. (a) Original image. (b) Segmented image.

The second experiment involves the detection of aneurysms in ultrasound images. The search algorithm is illustrated in this experiment, where an aneurysm is detected in two images regardless of template rotation and slight scale change. The two segmented ultrasound images are shown in Figure 3.

The third experiment involves the segmentation of cardiac MRI images. The two images of the heart were segmented using the same template, illustrating the warping capability as well as rotation invariance. This is shown in Figure 4.

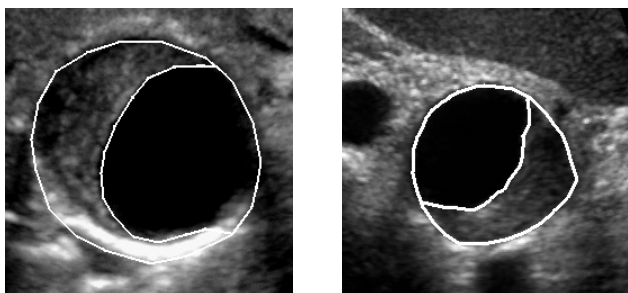


Fig. 3. Segmentation of Aneurysms in ultrasound images.

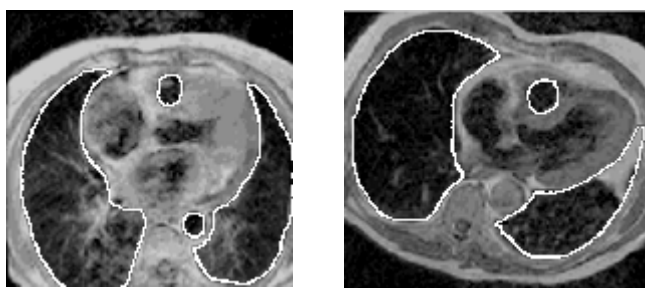


Fig. 4. Cardiac MRI segmentation.

The final experiment involves the detection of Carpal bones in x-ray images. This experiment shows how the algorithm can be adapted to object-tracking tasks. X-ray images were taken of the hand and wrist moving in an arc. In each consecutive image, the final template from the previous image is used as the initial template for the current image. In this way, full localization is not required, thus improving speed and computational efficiency. Figure 5 shows the x-ray images, clockwise in consecutive order.

## V. CONCLUSION

This paper presents a systematic approach to segmentation of medical images using deformable templates. Prototype templates capture typical object structure, and are then used to localize similar structures within an image. The method utilizes a multi-stage, multi-resolution algorithm to achieve computational efficiency. The algorithm begins by identifying regions of interest in the image, and proceeds to search these regions at progressively finer resolutions. Once

an object is located, the template is deformed to fit it using a particle swarm optimized, LWM warp routine. Experimental results have been presented showing invariant localization of objects in MRI, x-ray and ultrasound images.

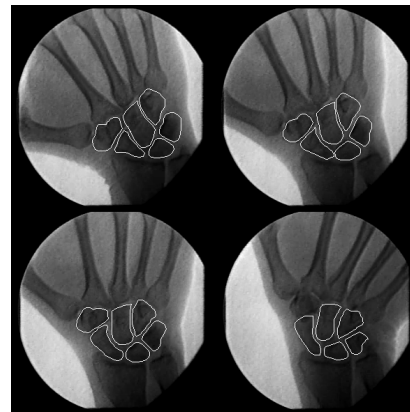


Fig. 5. Carpal Bone Segmentation from X-ray

## REFERENCES

1. Jain A K, Zhong Y, Lakshmanan S. (1996) Object matching using deformable templates. *IEEE Transactions on Pattern Analysis and Machine Intelligence*, 18(3):267–277
2. Grenander U. (1976) *Pattern synthesis: Lectures in pattern theory. Applied Mathematical Sciences (18)*. Springer-Verlag
3. McInerney T, Terzopoulos D. (1996) Deformable Models in Medical Image Analysis: A Survey. *Medical Image Analysis*, 1(2):91–108
4. Matlab Function Reference: Conv2. Matlab Signal Processing Toolbox, at: [www.mathworks.com/access/helpdesk/help/techdoc/ref/conv2.html](http://www.mathworks.com/access/helpdesk/help/techdoc/ref/conv2.html) Last date of access: 05-11-2005
5. Canny J. (1986) A Computational Approach to Edge Detection. *IEEE Transactions on Pattern Analysis and Machine Intelligence*, 8(6): 679–698
6. Kennedy J, Eberhart R C. (1995) Particle swarm optimization. *IEEE International Conference on Neural Networks*, 1(1):1942–1948
7. Goshtasby A. (1988) Image registration by local approximation methods. *Image and Vision Computing*, 6(4):255–261
8. Zagorchev C, Goshtasby A. (2006) A Comparative Study of Transformation Functions for Nonrigid Image Registration. *IEEE Transactions on Image Processing*, 15(3):529–538
9. Tagare Medical Image Database, National Library of Medicine, Yale University, USA.

Address of the corresponding author:

J.M. Spiller  
 School of Electrical & Information Engineering  
 Private Bag 3, University of the Witwatersrand  
 Johannesburg, Wits 2050  
 South Africa  
[j.spiller@ee.wits.ac.za](mailto:j.spiller@ee.wits.ac.za)